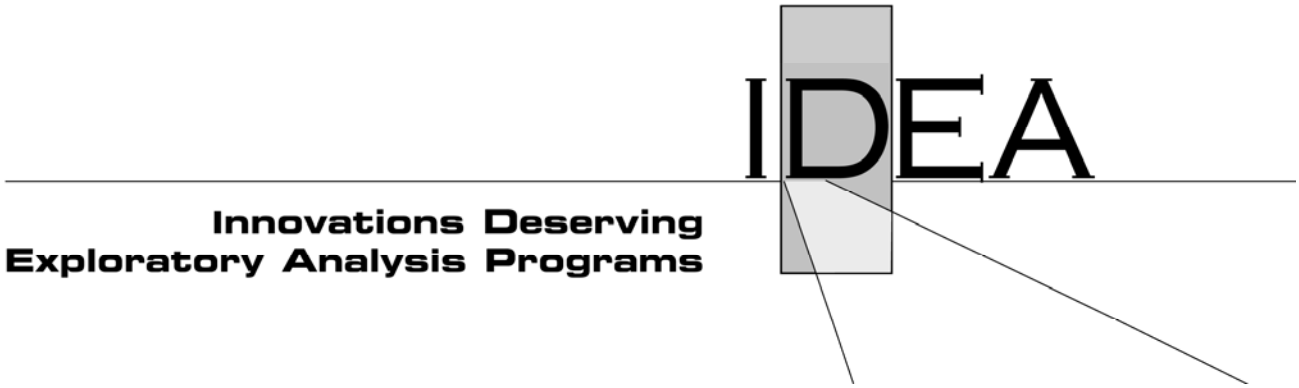

Highway IDEA Program

Development of a Simple Test to Determine the Low Temperature Creep Compliance of Asphalt Mixtures

Final Report for Highway IDEA Project 133

Prepared by:
Mihai Marastean, Raul Velasquez and Augusto Cannone Falchetto,University of Minnesota
Adam Zofka, University of Connecticut

June 2009

TRANSPORTATION RESEARCH BOARD
OF THE NATIONAL ACADEMIES

INNOVATIONS DESERVING EXPLORATORY ANALYSIS (IDEA) PROGRAMS MANAGED BY THE TRANSPORTATION RESEARCH BOARD (TRB)

This NCHRP-IDEA investigation was completed as part of the National Cooperative Highway Research Program (NCHRP). The NCHRP-IDEA program is one of the four IDEA programs managed by the Transportation Research Board (TRB) to foster innovations in highway and intermodal surface transportation systems. The other three IDEA program areas are Transit-IDEA, which focuses on products and results for transit practice, in support of the Transit Cooperative Research Program (TCRP), Safety-IDEA, which focuses on motor carrier safety practice, in support of the Federal Motor Carrier Safety Administration and Federal Railroad Administration, and High Speed Rail-IDEA (HSR), which focuses on products and results for high speed rail practice, in support of the Federal Railroad Administration. The four IDEA program areas are integrated to promote the development and testing of nontraditional and innovative concepts, methods, and technologies for surface transportation systems.

For information on the IDEA Program contact IDEA Program, Transportation Research Board, 500 5th Street, N.W., Washington, D.C. 20001 (phone: 202/334-1461, fax: 202/334-3471, http://www.nationalacademies.org/trb/idea)

Development of a Simple Test to Determine the Low Temperature Creep Compliance of Asphalt Mixtures

IDEA Program Final Report

for the period January/2008 through June/2009

NCHRP-133

Prepared for the IDEA Program

Transportation Research Board

National Research Council

Mihai Marasteanu
Raul Velasquez
Augusto Cannone Falchetto
University of Minnesota

Adam Zofka
University of Connecticut

June 2009
Minneapolis, Minnesota

TABLE OF CONTENTS

EXECUTIVE SUMMARY

CHAPTER 1
IDEA PRODUCT, CONCEPT, AND INNOVATION 1

CHAPTER 2
PREPARATION OF THIN ASPHALT MIXTURE BEAM 2
2.1 BEAM PREPARATION 2
2.1.1 TALL GYRATORY CYLINDER (170 ±2 MM HEIGHT BY 150 MM DIAMETER) 2
2.1.2 NORMAL GYRATORY CYLINDER (115 ±5 MM HEIGHT BY 150 MM DIAMETER) 3
2.1.3 FIELD CORES 3
2.2 STATISTICAL ANALYSIS OF THIN BEAM DIMENSIONS 3
2.3 CONCLUSIONS 4

CHAPTER 3
TESTING OF THIN ASPHALT MIXTURE BEAMS 5
3.1 LOADING PROCEDURE 5
3.1.1 DOUBLE STEP LOADING PROCEDURE 5
3.1.2 NORMAL LOADING PROCEDURE 6
3.1.3 PREDICT LOWEST TEMPERATURE CREEP STIFFNESS 6
3.2. OTHER FACTORS 7
3.2.1 COOLING MEDIUM 7
3.2.2 AIR VOIDS 7
3.3 CONCLUSIONS 8

CHAPTER 4
COMPARISON OF IDT AND BBR CREEP STIFFNESS EXPERIMENTAL DATA 9
4.1. MATERIALS 9
4.2. CREEP STIFFNESS CALCULATION 9
4.2.1 IDT – AASHTO PROCEDURE 9
4.2.2 BBR– THREE POINT BENDING THEORY 10
4.3. DATA ANALYSIS 10
4.4. HOMOGENEOUS MATERIAL TESTING AND DATA ANALYSIS 12
4.5. CONCLUSIONS 13

CHAPTER 5
REPRESENTATIVE VOLUME ELEMENT 14
5.1 TEST PROCEDURE 14
5.2 DATA ANALYSIS 15
5.3 CONCLUSION 16

CHAPTER 6
FINITE ELEMENT SIMULATIONS AND COMPOSITE MATERIALS MODELS 17
6.1. FINITE ELEMENT SIMULATIONS 17
6.2 COMPOSITE MATERIALS MODELS 21
6.2.1 HIRSCH MODEL 22

CHAPTER 7
BACK-CALCULATION OF ASPHALT BINDER CREEP COMPLIANCE.....24

CHAPTER 8
CONCLUSION, PLANS FOR IMPLEMENTATION, AND RECOMMENDATIONS FOR FURTHER RESEARCH 27
8.1 CONCLUSIONS.....27
8.2 PLANS FOR IMPLEMETATION 28
8.3 RECOMMENDATIONS FOR FURTHER RESEARCH 28

REFERENCES 29
APPENDIX.....31

LIST OF TABLES

TABLE 1 Load Levels to Obtain Tensile Strains of 60μstrains 6
TABLE 2 Lab Mixtures 9
TABLE 3 Field Mixtures 9
TABLE 4 Variables Definition for Statistical Analysis 11
TABLE 5 General Properties of HDPE and UHMW 12
TABLE 6 ANOVA for IDT Creep Stiffness 13
TABLE 7. Variables Definition for Statistical Analysis 15
TABLE 8 Correlation Factors for all Temperatures 16
TABLE 9 ANOVA for all Temperatures 16
TABLE 10 GMM Inputs for ABAQUS 17
TABLE 11 Corrected Values of VMA for Different Volume Ratios of Aggregates 26

LIST OF FIGURES

FIGURE 1 IDT and BBR test specimens 1
FIGURE 2 Cutting BBR mixture beams 2
FIGURE 3 Specimen holder for saw cutting in Step 2 3
FIGURE 4 Bending Beam Rheometer with thin asphalt mixture 3
FIGURE 5 Basic statistics for measured BBR mixture beams thickness 4
FIGURE 6 Double step loading in BBR 5
FIGURE 7 Error between experimental and predicted creep stiffness for PG 58-34 asphalt mixture 6
FIGURE 8 Comparison of different cooling medium 7
FIGURE 9 Sensitivity of Hirsch model to air voids 7
FIGURE 10 IDT creep stiffness versus BBR creep stiffness – PG 58-40, modifier 1 11
FIGURE 11 IDT versus BBR creep stiffness – all mixtures 11
FIGURE 12 IDT vs. BBR creep stiffness UHMW and HDPE plastic materials 12
FIGURE 13 1x, 2x, and 3x asphalt mixture beam specimens 14
FIGURE 14 2x and 3x mixture beam test setup 14
FIGURE 15 Test results for modified PG 64-28 mixtures 15
FIGURE 16 Generalized Maxwell model in parallel 17
FIGURE 17 IDT and BBR mesh in ABAQUS 18
FIGURE 18 Comparison of IDT and BBR simulations using FEM 18
FIGURE 19 2D and 3D beam structures 19
FIGURE 20 Example of processed 2D image using DIP 19
FIGURE 21 Extreme E_{mix} data points for V_{agg}=0.70 19
FIGURE 22 Weak (right) and strong (left) beam structures (V_{agg}=0.70) 20
FIGURE 23 E_{ma} as a function of E_{mix} for strong and weak beam structure 20
FIGURE 24 J_{ma} predictions for strong and weak beam structure 20
FIGURE 25 Semi-empirical model proposed by *Christensen et al. (44)* 22
FIGURE 26 Hirsch model predictions using, a) original *Pc*, b) proposed *Pc* 23
FIGURE 27 Hirsch model predictions with proposed *Pc*, a) -24°C, b) -36°C 23
FIGURE 28 Simplified mixture stiffness function 24
FIGURE 29 Comparison of experimentally obtained and back-calculated stiffness curves at -24ºC. 24
FIGURE 30 Simplified mixture stiffness function (Granite and Limestone) 25
FIGURE 31 Comparison of experimental and back-calculated creep stiffness, PG 58-28:U1 at -18ºC 25

EXECUTIVE SUMMARY

The idea of performing creep tests on asphalt mixture beam specimens with the Bending Beam Rheometer (BBR) was investigated in this project. In the first part of the investigation a detailed beam preparation procedure was developed for both laboratory compacted and field cores. The method was found to produce very uniform BBR mixture beams. For accurate results, the beams need to be measured before the one hour isothermal storage and the correct beam thickness and width need to be input in the test software.

A detailed loading procedure was developed and it was determined that good results can be obtained using the current BBR device at (PG low temperature + 22˚C) and (PG low temperature + 10˚C), respectively. At the lowest test temperature of (PG low temperature - 2˚C), it is recommended to predict the creep stiffness from the data obtained at the higher two temperatures and from time-temperature superposition. The cooling medium and reasonable variations in air voids do not significantly affect asphalt mixture creep stiffness results at low temperature.

Based on BBR and IDT experimental data for 20 laboratory mixtures a simple linear relationship was obtained between the IDT creep stiffness and the BBR creep stiffness obtained at (PG low temperature + 22˚C) and (PG low temperature + 10˚C). A similar relation could not be identified for the field samples. Differences of less than 3% were observed between IDT creep stiffness and BBR creep stiffness for two polymeric materials.

The representative volume element (RVE) of asphalt mixtures at low temperatures was investigated by performing three-point bending creep tests on beams of three different sizes. The statistical analysis of the 1x, 2x and 3x beams experimental data indicated that BBR asphalt mixture beams (1x) are an RVE of the material for (PG low limit + 22˚C) and (PG low limit + 10˚C). At the lowest test temperature (PG low limit - 2˚C), a robust analysis could not be performed due to the variability of the results due to the difficulties associated with testing the 2x and 3x beams.

The Finite Element simulations for a homogeneous asphalt mixture produced similar results for IDT and BBR, within 4% of each other, similar to the experimental results for two polymeric materials. Additional simulations indicated that aggregate spatial distribution in asphalt mixtures is very important and aggregate structure within the mixture should be taken into account when using an inverse model to predict the properties of the mixture components.

A number of micromechanics models were also evaluated. It was found that the modified Hirsch model is the most promising predictive model and its use in backcalculating the binder properties was analyzed. A simple algorithm, previously developed, was applied to the experimental data and the results, although reasonable, indicated that further investigation was needed to better predict the component asphalt binder creep stiffness from mixture testing.

A draft specification for obtaining low temperature creep stiffness of asphalt mixtures using the BBR was developed and will be presented at the next Asphalt Mixture ETG meeting in September for further comments. A draft specification will be submitted to ASTM by the end of the year with support from Georgia Department of Transportation Materials and Research Engineer, and Minnesota Department of Transportation and Utah Department of Transportation Asphalt Engineers.

CHAPTER 1

IDEA PRODUCT, CONCEPT, AND INNOVATION

Good fracture properties are an essential requirement for asphalt pavements built in the northern part of the US and in Canada for which the prevailing failure mode is cracking due to low-temperature shrinkage stresses. The current Superpave specifications address this issue through strength and creep tests performed on asphalt binder and asphalt mixture specimens.

For asphalt binders, Bending Beam Rheometer (BBR) tests are performed according to *AASHTO T313-08* (*1*) to obtain the lower limit of the performance grade (PG). Low-temperature creep tests are performed on thin beams of asphalt binders conditioned at the desired temperature for 1 hour. Based on the elastic solution for a simple supported beam and the correspondence principle that relates the governing field equations of elasticity and the Laplace transforms with respect to time of the basic viscoelastic field equations, the creep compliance is obtained. The final results are reported in the form of a plot of the inverse of the creep compliance, used as surrogate stiffness, versus time. The stiffness (*S*) and the m-value, which represents the slope of the log stiffness as a function of log time, are used to determine a critical temperature value based on limiting the stiffness obtained at 60 seconds to values lower than 300MPa and the m-value obtained at 60 sec to values higher than 0.300.

For asphalt mixtures, the Indirect Tension Tester (IDT) is used to perform creep and strength tests on cylindrical specimens loaded in compression along the diameter according to *AASHTO T322-07* (*2*). Asphalt mixture testing requires the use of expensive loading frames and expensive extensometers, which also require expensive and time consuming calibration and maintenance activities.

This project investigates the idea of performing creep tests on asphalt mixture beam specimens with the Bending Beam Rheometer (BBR). The BBR testing procedure has a number of important advantages:

- The instrument has a reasonable price and many laboratories have this instrument
- The BBR has a well documented history of good performance
- The BBR has a user friendly calibration verification
- The test procedure is very simple and the repeatability of the test results is very high.

This method can also be used to investigate the effect of surface aging, microcracking, and compaction on the mechanical properties of asphalt pavements by testing thin layers of asphalt mixtures recovered from different depths, which is not possible with the current IDT procedure, see Figure 1.

FIGURE 1 IDT and BBR test specimens

Furthermore, it can be used to improve the mix design of asphalt pavements built with RAP by providing a method to assess the effective properties of the binder, and to investigate the effectiveness of various surface treatments.

The next six chapters detail the steps taken to develop the IDEA product. Chapters 2 and 3 describe the work performed to develop the specimen preparation procedure and the loading procedure for thin mixture beam testing. Chapters 4, 5 and 6 provide comparisons of the IDT and BBR experimental data and the analyses based on composite material theories and finite element method. Chapter 7 addresses the issue of back-calculating the asphalt binder creep compliance from mixture testing.

The conclusions and the plans for implementation are discussed in Chapter 8.

CHAPTER 2

PREPARATION OF THIN ASPHALT MIXTURE BEAM

2.1 BEAM PREPARATION

Based on previous work (*3*) and laboratory work performed as part of this research, an improved procedure was developed to obtain asphalt mixture BBR beams. The procedure details how to obtain mixture thin beams from gyratory compacted specimens (2.1.1 and 2.1.2) and from field cores (2.1.3).

2.1.1 Tall Gyratory Cylinder (170 ±2 mm Height by 150 mm Diameter)

This method is used when other tests, such as IDT are performed and a comprehensive direct comparison of the BBR and IDT results is needed.

Step 1. The top 15 mm and the bottom 15 mm of the gyratory specimen are removed using a typical laboratory saw for mixture specimen preparation to obtain smooth surfaces. The remaining cylinder is cut into three 40 mm-thick IDT specimens, which are tested at three different temperatures (each at one temperature) to determine the mixture creep compliance (Figure 2).

Step 2. One day after IDT creep testing was completed, the specimens are further cut to obtain BBR thin beams. First, a thin slice, approximately 5 mm thick, is cut from one face of the IDT specimen to ensure a smooth surface and to remove any glue remaining from IDT buttons. Next, a 12.5 mm thick slice is cut from the remaining part of the IDT specimen. This slice is used in the next two steps to prepare the BBR beams. Note that the remaining 17-18 mm part at the bottom of the IDT specimen is necessary to hold the IDT specimen during saw cutting (see Figure 3) to remove the first thin layer and then accurately cut the next slice used for the BBR beams.

Step 3. The 12.5 mm thick slice is further cut from three sides to obtain 122 mm wide irregular slice.

Step 4. The slice obtained in step 3 is further cut into approximately 11 beams depending on the saw blade thickness.

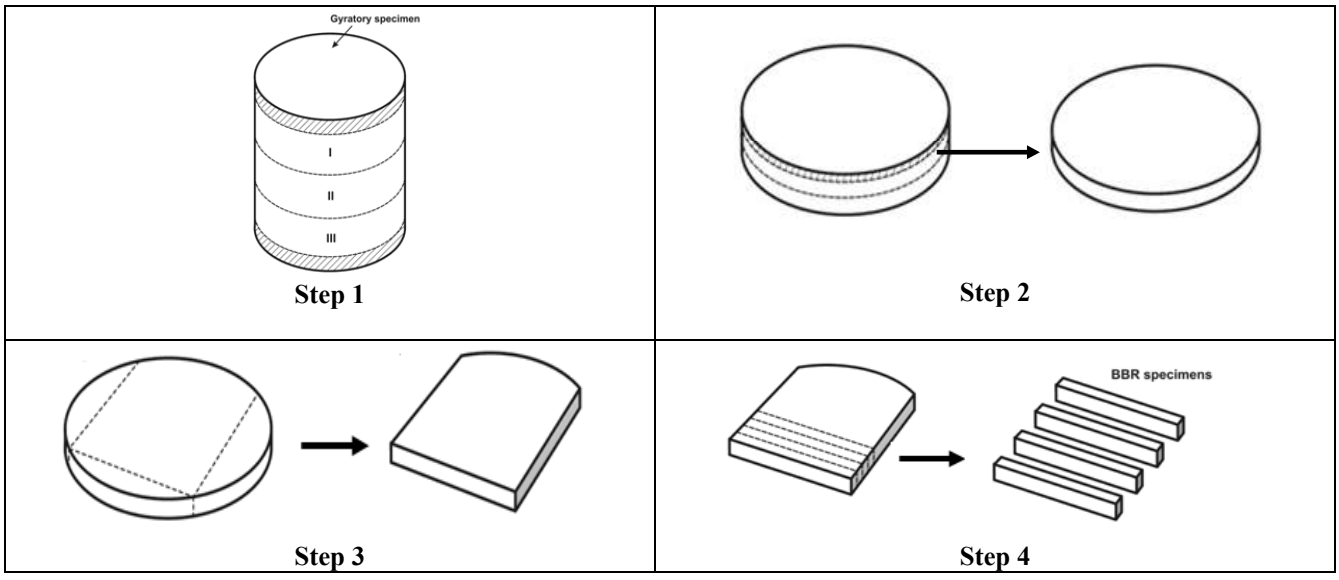

FIGURE 2 Cutting BBR mixture beams

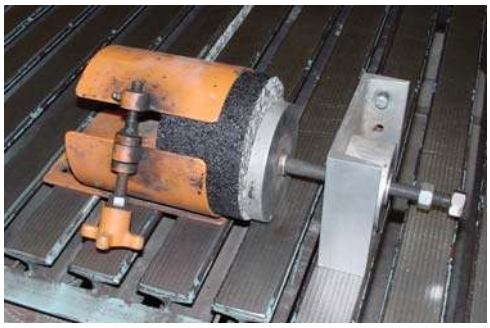

FIGURE 3 Specimen holder for saw cutting in Step 2

A simple tile saw with a continuous rim blade is used to produce BBR mixture beams with uniform dimensions (Figure 4). The experimental data suggests that the direction used to cut the thin beams with respect to the IDT specimens loading direction is not significant.

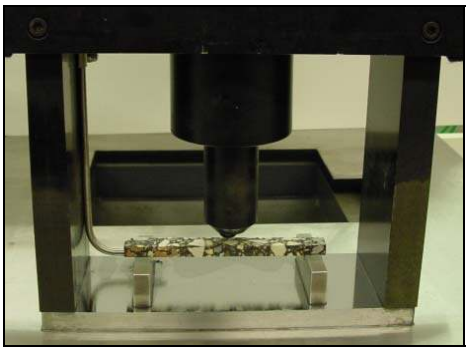

FIGURE 4 Bending Beam Rheometer with thin asphalt mixture

2.1.2 Normal Gyratory Cylinder (115 ±5 mm Height by 150 mm Diameter)

If IDT samples are required, then step 1 is modified as follows: the top 10 mm and the bottom 10 mm of the gyratory specimen are removed and the remaining cylinder is cut into two 40 mm-thick IDT specimens. The remaining steps do not change.

If other mechanical tests are not required, then step 1 is modified as follows: the top 45 mm of the gyratory is removed and a 12.5 mm thick slice is cut from the remaining cylinder; this slice represents the middle portion of the original gyratory specimen. The remaining steps do not change.

2.1.3 Field Cores

In this case, the cores should be cut into slices following the procedure previously described, taken into consideration that typical lift thickness is 50.8 mm (2 in.) Particular attention should be given to the core surface; for very rough surfaces, the top 5 mm may have to be removed; for reasonable smooth surfaces, the top can be kept since it represents the most aged portion of the asphalt pavement.

2.2 STATISTICAL ANALYSIS OF THIN BEAM DIMENSIONS

The procedure described was used to cut a total of 660 thin beams representing 11 replicates of 20 mixtures that were tested at three temperatures: (low temperature grade of binder + 10˚C) + 12˚C, (low temperature grade of binder + 10˚C), and (low temperature grade of binder + 10˚C) - 12˚C. A description of the mixtures is given in section 4.1

The thickness and width of the thin beams were measured at three locations along the length of the beam and average values were calculated. A standard laboratory caliper (Mitutoyo) was used to measure the dimensions of the beams, the device has a measuring range of 0-150 mm with a minimum indication (sensitivity) of 0.01 mm The dimensions of the beams are very consistent along the beam specimens. The average coefficient of variation for the thickness and width of individual beams are 2.12% and 1.23%, respectively. A summary of basic statistic parameters of the measured thin beams thickness values, which represents the most critical parameter in the calculation of creep compliance, is shown in Figure 5. Measured values of thickness ranged from 5.31 to 6.57 mm with a 2.43% coefficient of variation. The distribution of the thickness values shown in Figure 5 indicate that the values are normally distributed. Confidence intervals show that there is no large variation of the thickness values of the thin beams obtained with the proposed procedure.

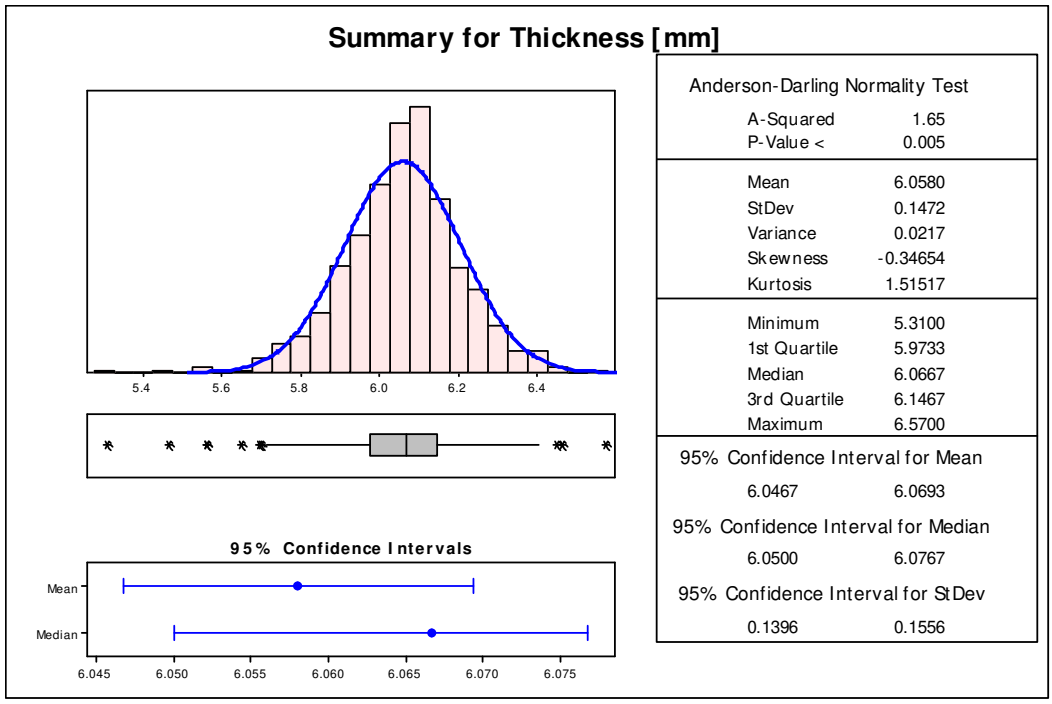

FIGURE 5 Basic statistics for measured BBR mixture beams thickness

The width of the thin beams is also normally distributed with a low coefficient of variation of 0.98%. Width measured values varied from 12.02 to 12.90 mm, and 95% confidence intervals for the width of the beams indicate that variation of this dimension among all the thin beams is not significant. To obtain accurate results, the beams need to be measured before the one hour isothermal storage and the correct beam thickness and width need to be input in the test software.

2.3 CONCLUSIONS

Based on the preparation of 660 thin beams, it was found that uniform BBR mixture beams can be produced by using a tile saw and following the steps described in this Chapter. The average coefficient of variation of the thickness and width for the thin beams are very small and indicate that the beams had very similar sizes.

CHAPTER 3

TESTING OF THIN ASPHALT MIXTURE BEAMS

3.1 LOADING PROCEDURE

BBR is used to perform creep tests on asphalt binder beams, see *AASHTO T 313-08* (*1*). Asphalt mixtures are one order of magnitude less compliant compared to asphalt binders at low temperatures and the challenge is to apply sufficient load to obtain measurable deflections of the mixture beams. The first tests, which followed strictly the asphalt binder testing protocol, generated very small deflections that could not be measured with reasonable resolution. Canon Instrument Company provided modified software that increased the resolution of the deflection measurements. The manufacturer also indicated that the standard BBR device can apply loads as high as 4413 mN without any change in the air bearing system. Note that the load cell capacity is 9806 mN; however, no compliance calibration was performed above the 4413 mN limit of the air bearing system and as a consequence, the software does not record load values above this limit.

The binder specification requires creep tests with duration of 240 sec. The binder specification is based on creep stiffness and m-values reported at 60 sec. The stiffness is calculated from the deflection measured at 60 sec; however, the *m*-value is obtained by fitting a second order polynomial to the entire 240 sec log stiffness vs. log time curve and is a reflection of the entire test data although only the 60 sec value is reported. For mixture testing, it was decided to perform BBR creep tests with duration of 1000 sec to compare the BBR results to the IDT results.

Mixture creep stiffness varies significantly with temperature and different load levels need to be determined for each temperature. In this research, the levels were established to maintain beam deflections between two limits during the entire duration of the creep test: a lower limit, initially set to approximately 30 μm, to avoid noise in the beam deflection data; an upper limit set to approximately 5% of the beam thickness, which corresponds to a deflection of 300 μm, derived from the assumption of small deflections of the Bernoulli-Euler beam theory.

Three levels of temperature were used to take advantage of the IDT data obtained in a different project (*4*):

- High temperature level (low temperature grade of binder + 10˚C) + 12˚C
- Intermediate temperature level (low temperature grade of binder + 10˚C)
- Low temperature level (low temperature grade of binder + 10˚C) - 12˚C.

After preliminary testing, it was decided to use approximately 1961 mN at high temperature level, 4413 mN at intermediate temperature level and 7159 mN at low temperature level. The loads used at high and intermediate temperatures can be applied using the standard BBR device and software without any modifications. For low temperature level, the load cannot be applied automatically and three different approaches were investigated to address this problem.

3.1.1 Double Step Loading Procedure

The 7159 mN load required to obtain deflections larger than 30 μm at the lowest temperature level was applied using double step loading. This procedure starts by applying a small load of approximately 98 mN using the BBR device. Then, after a very short time (2-3 sec), a second load is manually applied by placing a dead load of 7061 mN on the loading tray of the loading shaft, as shown in Figure 6.

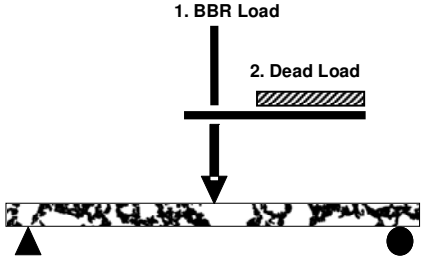

FIGURE 6 Double step loading in BBR

The dead load is a piece of steel of known weight that is gently placed on the loading tray to minimize dynamic forces. In this case, the deflection measurements need to be corrected to take into account the compliance of the system

for the load in excess of the 4413 mN that is not recorded by the BBR software. The corrections for compliance of the system were 3.53 and 3.70 μm per newton of load in excess of the 4413 mN at -30˚C and -36˚C, respectively.

The accuracy of this method was checked on a steel beam by measuring its elastic modulus using a load set only through BBR device and alternatively using the double step loading procedure. It was found that the difference between the elastic modulus calculated from both loading schemes was negligible. However, for viscoelastic materials loading history is very important and the timing of the second load has to be taken into account in the calculations.

3.1.2 Normal Loading Procedure

Further modifications of the BBR software by the manufacturer increased the resolution of deflection measurements; the latest hardware and software can resolve deflections of 0.15 microns with an accuracy of less than 1 micron. Preliminary testing indicates that if the maximum BBR load (4413 mN) is applied at the low temperature level reasonable deflection curves can be obtained, thus, avoiding the use of the double step loading procedure.

Note that the IDT creep procedure limits the tensile strains to values between 33 and 500 microstrains. The table below shows the load values required to obtain 60 microstrains for typical mixture stiffness values measured at the three temperature levels and 60s loading time. The following beam dimensions were assumed in the calculations: w = 12.7 mm, h = 6.35 mm, *span* = 101.6 mm.

TABLE 1 Load Levels to Obtain Tensile Strains of 60μstrains

Temperature Level	S@60s (GPa)	με	σ (MPa)	δ (μm)	Load (mN)	Load (g)
Low	20	60	1.20	16	4032	411.2
Intermediate	12	60	0.72	16	2419	246.7
High	5	60	0.30	16	1008	102.8

A limited number of comparisons of the double step applied after 2-3 sec from time zero and of the normal loading were performed. It was found that the average creep stiffness values obtained from the single and double step loading procedure are very similar. To further evaluate the difference, a test of hypotheses was performed to determine if there is any statistically significant difference between the means of the creep stiffness obtained with the two methods. No statistically significant differences were found between the results obtained with the two loading procedures.

3.1.3 Predict Lowest Temperature Creep Stiffness

In this approach, the intermediate and high temperature levels data is used to predict the creep stiffness at the lowest temperature level assuming time temperature superposition principle is valid. First, the creep stiffness data at the intermediate and high temperature are used to generate a master curve at the intermediate temperature using a modified *CAM* model (*5*), and to calculate the time shift factor between the high and intermediate temperatures. Then, assuming the same shift factor value between the intermediate and low temperature, the *CAM* model is used to predict the creep stiffness at the reduced times equivalent to the real loading times at the lowest temperature.

The results indicate that the prediction is reasonable. The error between the experimental data and the predicted creep stiffness varied between 2.66 and 9.68%, as shown in Figure 7.

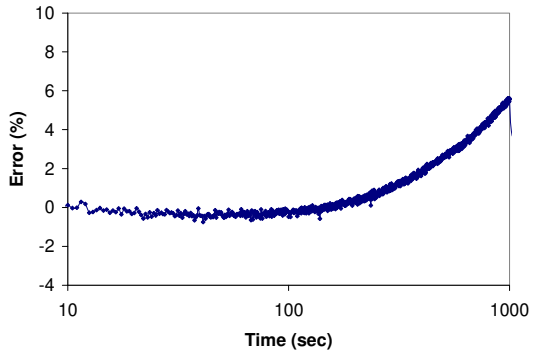

FIGURE 7 Error between experimental and predicted creep stiffness for PG 58-34 asphalt mixture

In conclusion, all three approaches provide similar results. However, taking into consideration that all tests were performed in a single laboratory by an experienced engineer, it is recommended that for specification purposes the third approach is followed to obtain the lowest temperature creep compliance.

3.2. OTHER FACTORS

Other factors can affect the results obtained with the IDT and BBR devices, respectively. The two main factors, the cooling medium, which is different in the two devices, and the air voids, which may be different in the two very different mixture specimens, were investigated.

3.2.1 Cooling Medium

Two asphalt mixtures were used to compare the creep stiffness obtained from thin beams tested with two cooling medium: air and alcohol. Testing in air was performed by placing the BBR loading frame into the Thermal Stress Restrained Specimen Test (TSRST) chamber and liquid nitrogen was used as cooling agent. Averages of the creep stiffness obtained by testing eleven replicates in air and in alcohol, respectively, are presented in Figure 8.

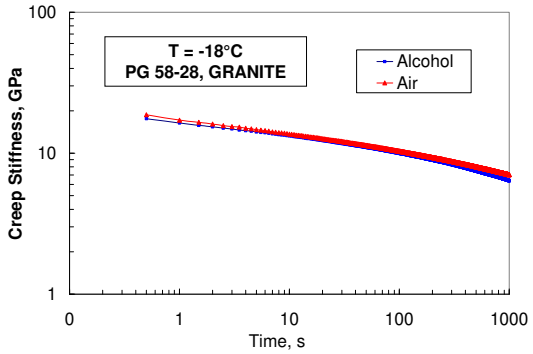

FIGURE 8 Comparison of different cooling medium

Further evaluation of the difference was performed with test of hypotheses. No statistically significant differences were found between the creep stiffness obtained from using air and alcohol as cooling medium. Although, on average the creep stiffness in air is 8% larger than the creep stiffness in alcohol, the repeatability of the BBR for asphalt mixtures varies between 4 and 13%.

3.2.2 Air Voids

The repeatability of the test results from multiple mixture beams suggests that differences in air void content among thin mixture beams do not significantly affect the creep compliance values. Air void measurement of individual thin mixture beams can be performed using an analytical balance and the standard procedure, according to researchers at Turner-Fairbank Highway Research Center asphalt laboratory. However, this approach needs to be further investigated and requires an expensive analytical balance. The standard procedures *AASHTO T 166-05* (*6*) and *AASHTO T209-05* (*7*) can be successfully used for the mixture slice from where the beams are cut. The measurements performed in this research indicate that the air voids in the IDT specimens and cylindrical slices from which the beams were cut were very similar.

Sensitivity analysis was performed using Hirsch model (*8*) described in detail in Chapter 6. Asphalt mixture creep stiffness values were predicted for a typical mixture with 0%, 2%, 4%, 6% and 8% air voids and are shown in Figure 9.

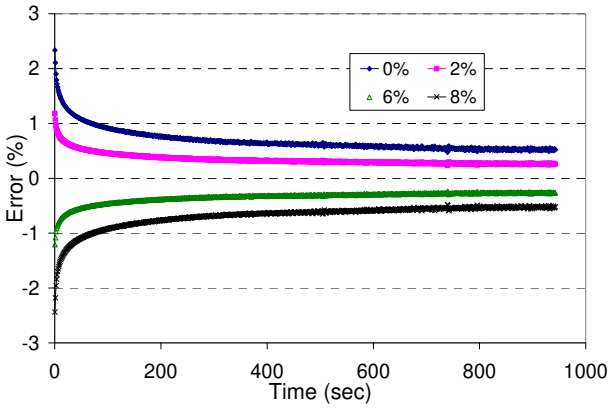

FIGURE 9 Sensitivity of Hirsch model to air voids

The results indicate that the differences between the creep stiffness of mixtures with different air void contents and the creep stiffness for the reference 4% air voids are very small.

3.3 CONCLUSIONS

Based on preliminary tests of thin asphalt mixture beams, good results can be obtained using the current BBR device and test loads of 1961 mN and 4413 mN at high (PG low temperature + 22˚C) and intermediate low temperature levels (PG low temperature + 10˚C) respectively. For the lowest temperature level (PG low temperature - 2˚C), the creep stiffness can be predicted from the data obtained at the higher two temperatures and from time-temperature superposition.

It was also found that the cooling medium and difference in air voids do not significantly affect asphalt mixture creep stiffness results at low temperature.

CHAPTER 4

COMPARISON OF IDT AND BBR CREEP STIFFNESS EXPERIMENTAL DATA

4.1. MATERIALS

One of the main objectives of this investigation was to determine if BBR experimental results match the IDT results. Experimental data obtained for 20 laboratory mixtures that consist of combinations of aggregate type, binder type, air voids, and asphalt content and field cores from 4 pavements (Table 2 and 3) were used in the analysis.

TABLE 2 Lab Mixtures

Air Voids →		Design (4%)	
Aggregate type		Aggregate 1 – Granite	Aggregate 2 - Limestone
Binder Type (modification)	PG58-40, modifier 1	X	X
	PG58-34, modifier 1	X	X
	PG58-34, modifier 2	X	X
	PG58-28, plain 1	X	X
	PG58-28, plain 2	X	X
	PG64-34, modifier 1	X	X
	PG64-34, modifier 2	X	X
	PG64-28, plain 1	X	X
	PG64-28, modifier 1	X	X
	PG64-22, plain	X	X

TABLE 3 Field Mixtures

MnROAD: Cell 03 - PG 58-28
MnROAD: Cell 19 - PG 64-22
WI US-45 - PG 58-34
WI STH-73 - PG 58-28

The laboratory mixtures were prepared with four different asphalt binder grades, and two types of aggregate: limestone and granite. They were compacted to 4% air voids using a gyratory compactor and following the Superpave mix design procedure. Nominal maximum aggregate size (NMAS) was 12.5 mm for all laboratories mixtures. For the MnROAD field mixtures the NMAS was 12.5mm, and for the Wisconsin mixtures it was 19.5mm.

4.2. CREEP STIFFNESS CALCULATION

IDT and BBR tests were performed according to *AASHTO T 322-07* (*2*) and BBR mixture tests were performed according to *AASHTO T313-08* (*1*) and using the loading levels described in Chapter 3. Tests were performed at three temperature levels, as described in 3.1. The creep stiffness values were calculated as follows.

4.2.1 IDT – AASHTO Procedure

The displacement and the load measured during creep tests in Indirect Tensile (IDT) are used to calculate the creep compliance *D* of asphalt mixtures. Roque and Buttlar (*9*) proposed the AASHTO method (*AASHTO T 322-07* (*2*)) that is based on Frocht solution (*10*) for stress distributions along horizontal and vertical axes in IDT test. Creep compliance *D* for the plane stress conditions is derived from Hooke's law by using elastic-viscoelastic correspondence principle (*11*):

$$D(t) = \frac{\varepsilon_x}{\sigma_x - \nu\sigma_y} \quad [1]$$

In order to take into account various phenomena during testing, several corrections coefficients *C* are introduced:

- C_{Bx}, C_{By} coefficients for bulging of specimen faces, applied to measured horizontal deformations H_M and vertical deformation Y_M, respectively.
- $C_{\varepsilon x}$, $C_{\varepsilon y}$ coefficients are used to convert average strain (derived from corrected deformations *H and Y*) to horizontal (and vertical) strain at a point in the middle of the specimen.
- C_{Sx}, C_{Sy} coefficients are used to convert 2D to 3D solution. They are applied to 2D stress solution for σ_x and σ_y, respectively.

The final expression for *D(t)* is written as:

$$D(t) = \frac{\Delta X \cdot D_{avg} \cdot b_{avg}}{P_{avg} \cdot GL} \cdot C_{cmpl} \quad [2]$$

ΔX – trimmed mean of the horizontal deformations,
D_{avg} – average specimen diameter,
b_{avg} - average specimen thickness,
P_{avg} – average force during the test,
GL – gage length (38mm)
C_{cmpl} – creep compliance parameter at any given time, computed as

$C_{cmpl} = 0.6354 \cdot \left(\frac{X}{Y}\right)^{-1} - 0.332$, where

X – measured horizontal deformation,
Y – measured vertical deformation.
D(t) – creep compliance,

According to *AASHTO T 322-07* (*2*) three temperatures (0°C, -10°C, -20°C) with three replicates at each temperature should be used in performing IDT. A *trimmed mean approach is used in the procedure*: the extreme values of displacements *X* and *Y* are removed and remaining values are averaged. The sorting is performed on measurements either in the middle of the creep test or on 'mid-test' averages taken from the time window between 460sec and 540sec.

4.2.2 BBR– Three Point Bending Theory

The Bernoulli-Euler law of elementary bending theory and the related differential equation of the deflection curve under arbitrary load can be written in the following form (*12*):

$$\frac{d\theta}{dx} = \frac{d^2v}{dx^2} = -\frac{M}{EI} \quad [3]$$

where θ is the angle of rotation, v is the beam deflection, M is the bending moment.

The main assumptions applied to derive Equation 3 are: plane sections remain plane, plane stress mode is valid, deflections v and angle θ are small and material is isotropic and linear. The Bending Beam Rheometer (BBR) load condition corresponds to a simply supported beam is loaded with one concentrated force at the midpoint of the span. The beam deflections δ at any distance x from one of the supports can be found, with appropriate boundary conditions, by employing the method of successive integrations. Applying this method to Equation 3, the maximum deflection δ_{max} that occurs at the midpoint of the span can be expressed by:

$$\delta_{max} = \frac{Pl^3}{48EI} \quad [4]$$

where l is beam span and P is a concentrated force.

Creep compliance *D(t)* can be obtained by means of Equation 5 and correspondence principle:

$$D(t) = \frac{48I\delta(t)}{Pl^3} \quad [5]$$

4.3. DATA ANALYSIS

Both visual inspection and statistical analyses were performed to compare the IDT and BBR creep stiffness experimental data.

An example of IDT creep stiffness plots and BBR creep stiffness plots for a single laboratory mixtures and different aggregate (granite and limestone) is shown in Figure 10.

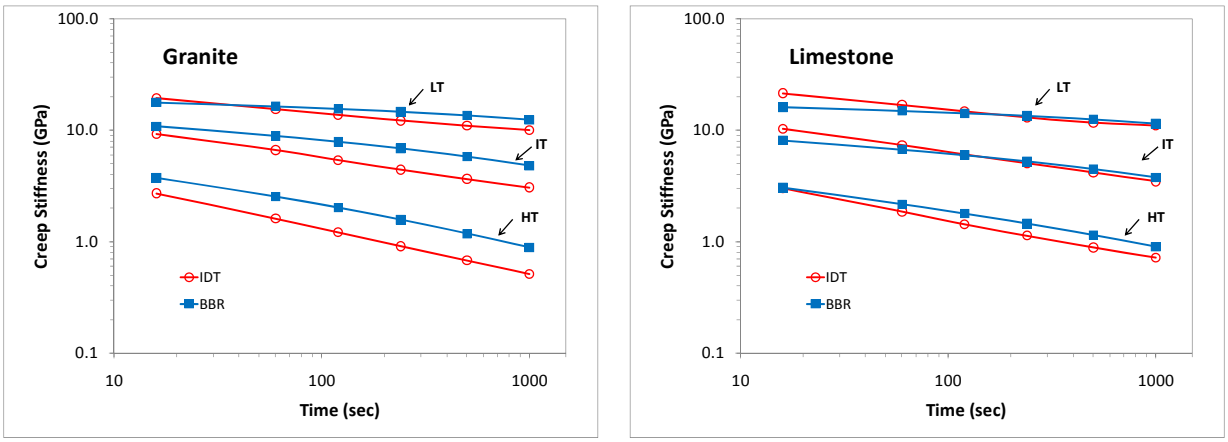

FIGURE 10 IDT creep stiffness versus BBR creep stiffness – PG 58-40, modifier 1

Figure 11 presents plots of the IDT creep stiffness versus BBR creep stiffness for all mixtures tested, all three temperature levels and six loading times (16s, 60s, 120s, 240s, 500s and 1000s). The values for the creep stiffness at high and intermediate temperature are generally below the line of equality and they concentrate in a narrow region. The stiffness points at low temperature are overall above the line of equality showing that for this temperature level the IDT creep stiffness is higher than BBR creep stiffness. The creep stiffness points measured at low temperature level are spread out more, an indication that testing at very low temperatures poses many difficulties. The field data is always above the line of equality, indicating that the IDT stiffness is always higher than BBR values. This pattern in the field specimens may be explained by the aging of the field samples.

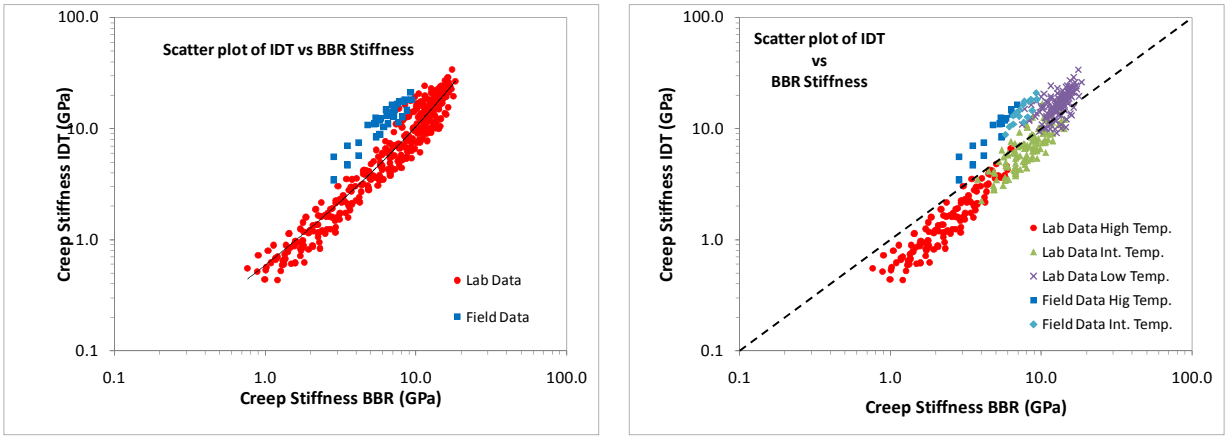

FIGURE 11 IDT versus BBR creep stiffness – all mixtures

The plot in Figure 11 suggests that for the laboratory data there is a linear relation between BBR and IDT creep stiffness. A number of analyses of variance (ANOVA) were performed using the creep stiffness as response variable and aggregate, temperature, test type and time as the independent parameters. A linear relation was assumed between response variable and the predictors. Statistical analysis was performed only on laboratory data and on creep stiffness values at 16, 60, 120, 240, 500 and 1000 seconds. Table 4 shows how the variables were treated in the statistical analysis.

TABLE 4 Variables Definition for Statistical Analysis

Independent Variable	Type / Description
Aggregate Type	0 – limestone ; 1 – granite
Temperature	High, intermediate, low level (different values)
Test Type	0 – IDT; 1 – BBR
Time	16, 60, 120, 240, 500 and 1000 sec

After many iterations, involving various models and combinations of the independent variables, it was found that a very simple model can be obtained using the experimental data obtained at the highest two levels of temperature and disregarding the lowest temperature results due to the higher degree of error associated with the high variability of the IDT data:

$$S_{IDT} = a \cdot S_{BRR} \qquad (a = 0.865) \qquad [6]$$

This expression indicates that, for the experimental data obtained in this research, at PG low temperature + 22˚C and PG low temperature + 10˚C, respectively, the IDT creep stiffness can be reasonably approximated as 86.5% of the BBR creep stiffness given the same loading time and test temperature.

4.4. HOMOGENEOUS MATERIAL TESTING AND DATA ANALYSIS

A similar comparison was performed on two polymeric materials to determine if the non-homogeneous nature of the asphalt mixtures is a significant factor in the IDT-BBR comparison. The materials selected, High-Density Polyethylene (HDPE) and Ultra-High Molecular Weight polyethylene (UHMW), are homogeneous at the macroscopic level and are viscoelastic at ambient temperature. The general physical and mechanical properties are shown in Table 5.

TABLE 5 General Properties of HDPE and UHMW

Property	HDPE	UHMW
Density [g/cm^3]	0.95	0.93
Tensile Strength [MPa]	32.0	21.4
Flexural Modulus [MPa]	1380.0	860.0
Hardness, Shore D	D69	D62-D66

Two blocks of HDPE and UHMW were used to cut IDT and BBR specimens: 38 × 305 × 305mm (UHMW) and 36 × 305 × 305mm (HDPE). Four IDT specimens of 142mm in diameter were cut from each block. Two IDT specimens from each material were used for testing. After testing, each IDT specimen was further cut into BBR beams. Using IDT and BBR, the creep stiffness for both materials was determined. Creep tests were performed at room temperature for 240sec. Specimen location within material block, load level and direction of load application were the three factors considered in testing. Figure 12 shows the plots of IDT vs. BBR in terms of creep stiffness for both UHMW and HDPE materials.

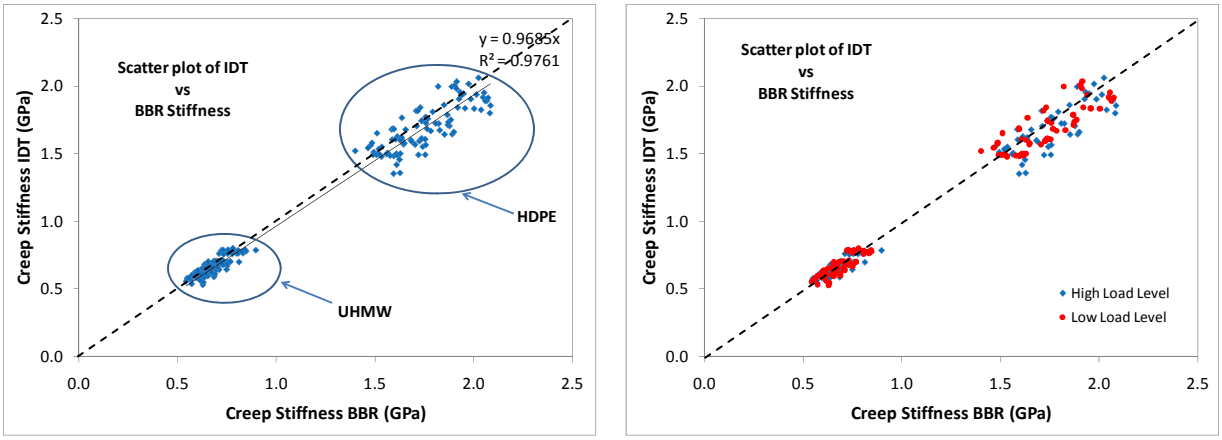

FIGURE 12 IDT vs. BBR creep stiffness UHMW and HDPE plastic materials

A linear relation seems to relate the data points with a slope coefficient slightly smaller than 1. In general, the values of the BBR are higher than the values of IDT. The influence of load level and time on the creep stiffness of plastic materials was investigated using correlation matrices and analyses of variance. A linear relation was assumed between the independent and dependent variables.

The results of ANOVA for the plastic materials are presented in Table 6. It is observed that only BBR creep stiffness is significant for a 5% significance level, and that IDT creep stiffness and BBR creep stiffness for the polymeric materials are almost identical since the coefficient that relates them is almost equal to 1 (0.971).

TABLE 6 ANOVA for IDT Creep Stiffness

Variable	Estimate	Std. Error	t-value	p-value
S BBR (GPa)	0.971	0.006	167.065	**0**
Load Level	-0.007	0.011	-0.651	0.516

4.5. CONCLUSIONS

A number of conclusions can be drawn from the IDT and BBR experimental data for asphalt mixtures and polymeric materials.

For asphalt mixtures, a simple linear relationship was obtained between the IDT creep stiffness and the BBR creep stiffness obtained at the intermediate and high temperature levels. IDT creep stiffness is approximately equal to 86.5% of the BBR creep stiffness. The IDT experimental data at the lowest temperature level is not always reliable, due to the formation of ice around extensometers and very small deformations, and was not included in the model. A similar relation could not be identified for the field samples, most likely due to the aging gradient in field cores.

For the two polymeric materials tested, differences of less than 3% were observed between IDT creep stiffness and BBR creep stiffness. This appears to indicate that a portion of the difference between the BBR and IDT data can be explained by the non-homogeneous nature of asphalt mixtures. It should be noted however, that at room temperature the stiffness of these materials is an order of magnitude lower than the creep stiffness of asphalt mixtures at the lowest temperature level.

CHAPTER 5

REPRESENTATIVE VOLUME ELEMENT

The main concern with using the BBR method for asphalt mixtures is the small size of the specimens that may not be representative of the asphalt pavement. Although the IDT-BBR analysis previously described indicates a linear relationship between the results from the two test methods, a more rigorous analysis is needed. In this section, the critical issue of the representative volume element (RVE) is investigated by performing three-point bending creep tests on beams of three different sizes. Ten of the laboratory mixtures described in Table 2 were tested for this purpose.

5.1 TEST PROCEDURE

Three-point bending creep tests were performed on specimens with three different sizes: 6.25 × 12.5 × 100 mm (1x, which represents the BBR specimen standard size), 12.5 × 25 × 200 mm (2x), and 18.75 × 37.5 × 300 mm (3x). Tests were performed at the same three temperature levels as before: high temperature (HT) level (PG low limit + 22˚C), intermediate temperature (IT) level (PG low limit + 10˚C), and low temperature (LT) level (PG low limit - 2˚C).

First, the slab compacted mixtures were cut into six 3x beams (Figure 13). Tests were performed at the three temperature levels HT, IT, and LT. After testing was finished, the 3x beams were cut into 2x beams using a water-cooled diamond saw. Bending tests were performed on the 2x beams using the test setup for 3x beams. After testing was completed, the 2x beams were cut into 1x beams the size of BBR specimens and tested in the BBR device.

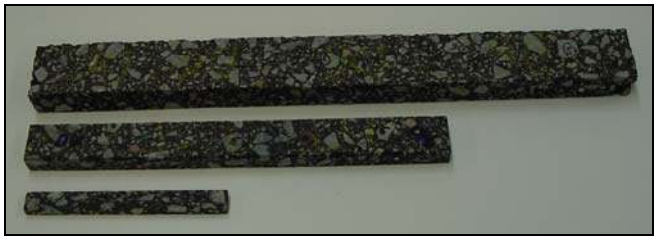

FIGURE 13 1x, 2x, and 3x asphalt mixture beam specimens

The test for 3x and 2x beams were conducted using a MTS 810 servo hydraulic testing machine. A special support manufactured in house was used to hold the beam and to measure mid span deflection and deformation of the beam at both ends of the support, as shown in Figure 14. The ends can be adjusted to different span lengths. The beam deflections were measured using Epsilon extensometers with 38 mm gage length and ±1 mm range.

FIGURE 14 2x and 3x mixture beam test setup

To eliminate the creep from the weight of the 2x and 3x beams, the deflection measured was considered as the sum of the deflection due to the load applied at the mid span and the deflection due to a uniformly distributed load equivalent to the weight of the beam. Due to the buoyancy forces in the BBR ethanol bath, the submerged weight for the 1x beams was negligible and not used in the calculations.

5.2 DATA ANALYSIS

A total of 360 tests were performed on the three different size beams at three temperatures. The creep stiffness as function of time was calculated using Bernoulli-Euler beam theory and the correspondence principle, as previously explained. For each asphalt mixture and temperature level, the average creep stiffness was calculated.

Figure 15 shows the creep stiffness curves for one of the asphalt mixtures tested. Visual inspection of the creep stiffness average curves for all ten mixtures indicates that, at intermediate and high temperature, the effect of the beam size is negligible. At low temperature the size of the beam appear to influence the creep stiffness. It is important to note that, during testing of the 2x and 3x beams at LT, the formation of layers of ice on the supports and around the extensometers was observed, similar to IDT testing. This may have influenced the deflection readings since the deflection values are very small at LT and the level of error in measurements is high compared to the other temperature levels.

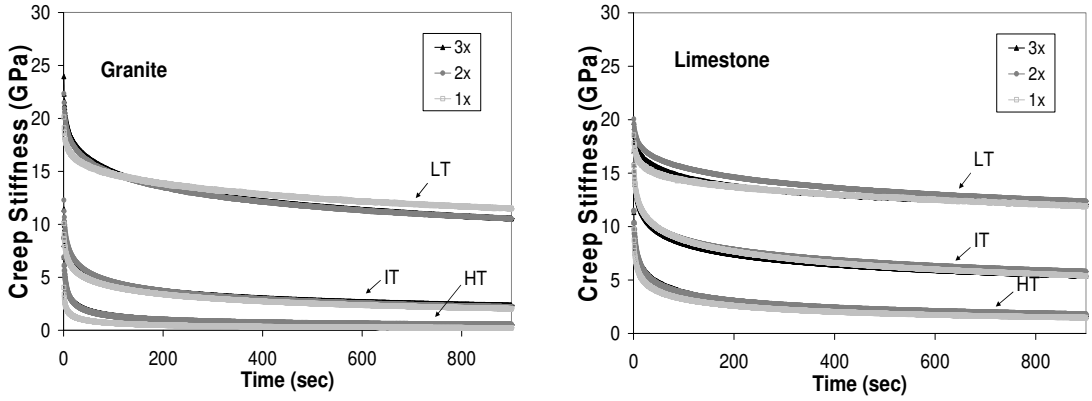

FIGURE 15 Test results for modified PG 64-28 mixtures

To further investigate the influence of parameters such as the size of the specimen, PG of the binder, aggregate type, loading time and temperature on the creep stiffness of asphalt mixtures, correlation matrices were calculated and analyses of variance (ANOVA) were performed using the creep stiffness as response variable and size, time, temperature, binder type, and aggregate as the independent parameters. A linear relation was assumed between response variable and the predictors. To reduce calculations, only the creep stiffness values at 8, 15, 30, 60, 120 and 240 seconds were used in the analysis. Table 7 shows how the variables were treated in the statistical analysis.

TABLE 7. Variables Definition for Statistical Analysis

Variable	Type / Description
Binder PG	Factors (dummy): PG 58-34, PG 58-28, PG 64-34, PG 64-28
Binder modification	0 – unmodified; 1 – modified
Aggregate Type	0 – granite; 1 – limestone
Beam size	1 - 1x beams; 2 - 2x beams; 3 - 3x beams
Time	8, 15, 30, 60, 120 and 240 sec

First, the analysis considered the results at both intermediate and high temperature levels. Then, separate analyses were performed for high and intermediate temperature levels. The creep stiffness data from the low temperature level was not included in the statistical analysis due to the high variability of the deflection measurements.

Correlation factors for the combined results at HT and IT are presented in Table 8. For the data set used in this analysis, correlations larger than 0.057 (n = 1225) are significant and presented in bold.

TABLE 8 Correlation Factors for all Temperatures

	Creep Stiffness
Aggregate	**0.128**
Modification	**-0.123**
Size	-0.037
Size*Aggregate	**0.095**
Size*Time	**-0.361**
Temperature	**-0.681**
Time	**-0.400**

The only parameter that has no significant correlation with creep stiffness is size. This indicates that there are no statistically significant differences between the creep stiffness functions of the 3x, 2x, and 1x beams. This is confirmed by ANOVA results presented in Table 9. For a significance level of 5%, the variables with p-values smaller than 0.05 are significant and presented in bold. The parameters in the regression that do not significantly contribute to the prediction of creep stiffness are size, aggregate type and the interaction terms between size, aggregate and time.

TABLE 9 ANOVA for all Temperatures

Variable	**Estimate**	**Std. Error**	**t-value**	**p-value**
Constant	3132.87	290.97	10.77	**0**
Size	-16.27	111.89	-0.15	0.884
Size*Aggregate	149.65	132.79	1.13	0.260
Size*Time	0.10	0.81	0.13	0.900
Binder[64-28]	1158.85	165.25	7.01	**0**
Binder[58-34]	288.82	240.86	1.20	0.231
Binder[64-34]	1934.80	249.58	7.75	**0**
Modified	-3601.87	165.05	-21.82	**0**
Aggregate	254.22	287.08	0.89	0.376
Temperature	-510.70	9.68	-52.75	**0**
Time	-19.73	1.74	-11.34	**0**

The analyses performed separately for the HT and IT temperature levels had the same outcome: no significant correlation was observed between creep stiffness and the size of specimens and the size of the specimens did not provide significant information for the prediction of the creep stiffness in the assumed linear models.

5.3 CONCLUSION

The results from this statistical analysis suggest that the thin BBR asphalt mixture beams are an RVE of the material for two of the temperatures used in the experimental investigation: PG low limit + 22˚C, and PG low limit + 10˚C. Note that "PG low limit + 10˚C" is the actual test temperature at which asphalt binders are tested to obtain the binder grade.

At the lowest temperature "PG low limit - 2˚C" a robust analysis could not be performed due to the variability of the results due to the difficulties associated with testing the 2x and 3x beams.

CHAPTER 6

FINITE ELEMENT SIMULATIONS AND COMPOSITE MATERIALS MODELS

The experimental results and analyses described in the previous chapters indicate that the IDT and BBR methods produce similar creep stiffness results. The influence of specimen geometry (IDT vs. BBR) and of the aggregate spatial distribution inside the BBR beam is further investigated by means of finite element modeling.

In addition, the mechanical response of the BBR asphalt mixture beams can be analyzed and predicted by micromechanical models. Selection of an accurate micromechanical model is critical in evaluating the contribution of the component phases of a composite material and in developing backcalculating algorithms to estimate these contributions from tests performed on the composite material. In this chapter, different micromechanical models were evaluated with respect to their ability to predict the effective properties of asphalt mixtures.

6.1. FINITE ELEMENT SIMULATIONS

Simulations of IDT and BBR creep tests were performed by means of ABAQUS software. Model geometries, such as specimen dimensions and load transfer devices, and the Generalized Maxwell Model (GMM), a built-in material model, were used to model asphalt mixtures as homogeneous, linear viscoelastic materials.

Since GMM is written for relaxation modulus and most micromechanical models describe modulus variation, it was necessary to convert the experimental creep compliance to relaxation modulus. A Generalized Voigt (Kelvin) mechanical model in series was used to simulate the creep behavior of binder and mixture, from which the Prony series coefficients for the relaxation modulus E represented by the Generalized Maxwell (Wiechert) model (Figure 16) are obtained:

$$E(t) = E_0 - E_1\left(1 - e^{-t/\rho_1}\right) - E_2\left(1 - e^{-t/\rho_2}\right) - E_3\left(1 - e^{-t/\rho_3}\right) \quad [7]$$

where

E_{inf} – log-time equilibrium modulus,

ρ_i – relaxation time,

E_i – modulus for spring i.

$$E_\infty = E_0 - \sum_{i=1}^{3} E_i \qquad \rho_i = \frac{\eta_i}{E_i} \quad [8]$$

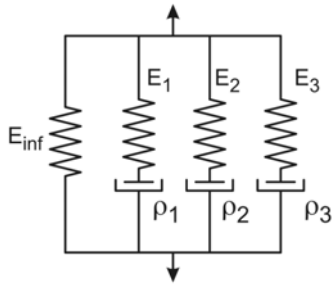

FIGURE 16 Generalized Maxwell model in parallel

The parameters used in the GMM model, such as shear g_i and bulk k_i relaxation moduli are given in Table 10. The following assumptions were made: the Poisson ratio v for asphalt mixture was assumed constant and equal to 0.3 (thus g_i=k_i); instantaneous elastic modulus E_0 for asphalt mixture was determined as 8.44 GPa.

TABLE 10 GMM Inputs for ABAQUS

Normalized shear relaxation modulus, g_i [-]	**Normalized bulk relaxation modulus, k_i [-]**	***Relaxation time,* ρ_i [sec]**
0.3542	0.3542	2.8889
0.2114	0.2114	33.0071
0.2417	0.2417	334.0924

The loading strips in IDT test were assumed to be made of an elastic, isotropic and homogenous material with Young modulus 300GPa and Poisson ratio 0.3. Full contact between asphalt mixture specimen and loading strips was assumed in IDT model since it has small influence on the state of stress around the center of the specimen (*9*).

In order to save computational time, only 1/8 of IDT specimen was considered (Figure 17) and the following parameters were used to model different combinations of IDT mesh density:

- element type,
- *CETOL* value (maximum difference in the creep strain over one time increment).

The best results in reasonable time were produced by the model containing 24010 wedge elements (C3D15) and when *CETOL* parameter is set to 1e-08 during the analysis. A simply supported beam with no overhanging parts was used to model BBR test. 7200 brick elements (C3D20R) were used in the beam mesh shown in Figure 17.

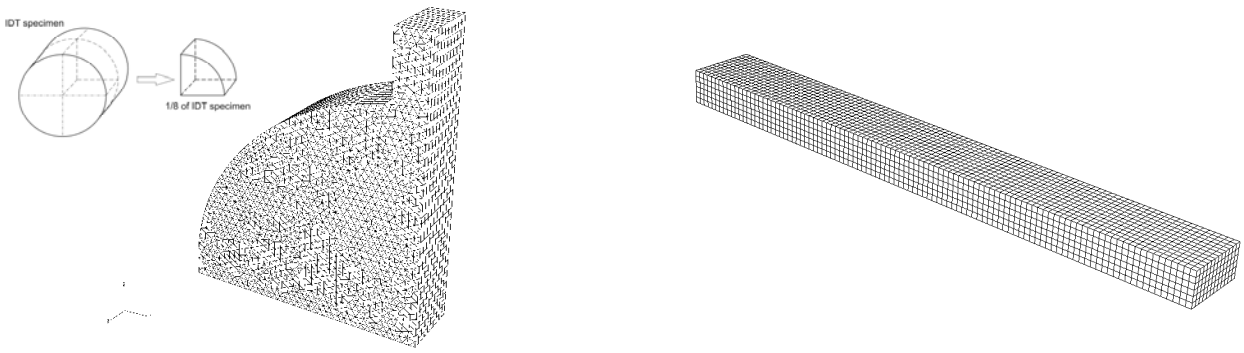

FIGURE 17 IDT and BBR mesh in ABAQUS

In order to simulate the creep tests, an instantaneous force was applied at time t = 0sec and kept for the following 10sec. The displacements of gauge points were obtained from ABAQUS output at appropriate nodes similar to IDT testing. For BBR, virtual beam deflections were recorded from neutral axis in the middle of the span and creep compliance *J(t)* was computed using Bernoulli-Euler beam theory.

The ratios between calculated *J(t)* using the IDT and BBR methods, respectively, and the ABAQUS material input (assumed as 'true' material response) were computed and are shown in Figure 18. Similar to the analysis of the polymeric materials experimental data, the simulations indicate that IDT and BBR produce similar results, within 4% of each other.

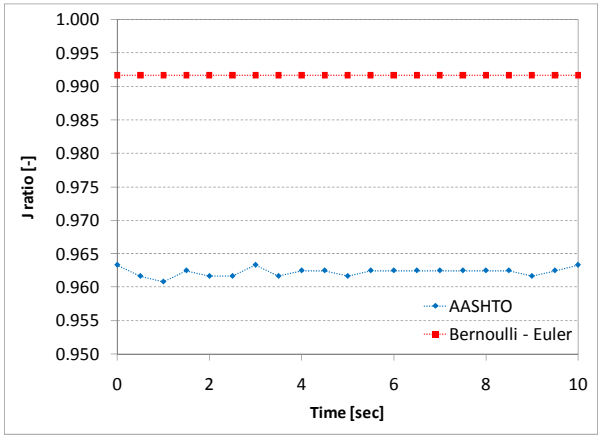

FIGURE 18 Comparison of IDT and BBR simulations using FEM

Additional simulations were performed to evaluate the effect of aggregate structure. In this case, the asphalt mixture structure was simulated as a 2-phase composite material: asphalt mastic and aggregates. A concentrate load of 280N was applied to the mid-span of a SSB with a length of 101.6mm and thickness of 5.588mm for the case of 2D ABAQUS simulations. The selected element used were square mesh elements, CPS8R (plane stress quadratic reduced integration element); the side length of this elements was 0.508mm. The "black" mesh elements correspond to asphalt mastic and the "white" to aggregate, see Figure 19. For 3D simulations, C3D20R brick elements were used.

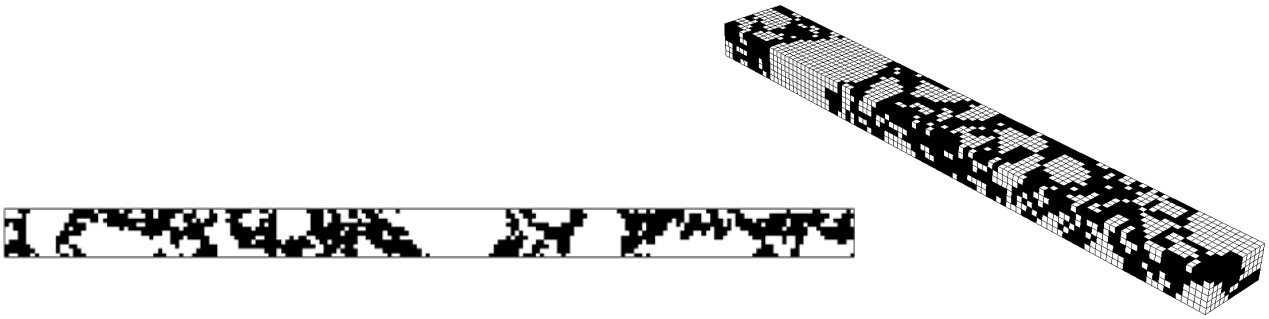

FIGURE 19 2D and 3D beam structures

The model was built up from digital images of BBR mixture beams obtained with a 2400dpi 8-bit scanner. Digital Image Processing (DIP) techniques were used to obtain the mastic and aggregate phases and included conversion of the original image to the binary image (black-and-white), filtering, and segmentation based on global thresholding. An example of raw 2D BBR face image and its processed version is shown in Figure 20.

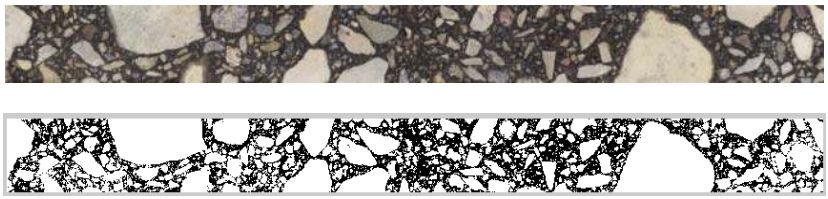

FIGURE 20 Example of processed 2D image using DIP

To investigate the influence of the aggregate skeleton structure, 350 different 3D beam structures were generated for the ABAQUS input model. The beams were subdivided in 7 groups of 50 beams each and assigned randomly to seven aggregate volume fractions V_{agg}: 0.40, 0.45, 0.50, 0.55, 0.60, 0.65, and 0.70. Ten 3D simulations were run for each beam changing the elastic modulus E_{ma} of the mastic phase: 0.1, 1, 2, 4, 6, 9, 12, 14, 16, and 18GPa. In all simulation, the aggregate elastic properties (E_{agg}=20GPa, v_{agg}=0.3) and mastic Poisson ratio (v_m=0.3) were assumed constant. Figure 21 shows the values for V_{agg}=0.70 of the effective modulus E_{mix} that was calculated using Bernoulli-Euler beam theory.

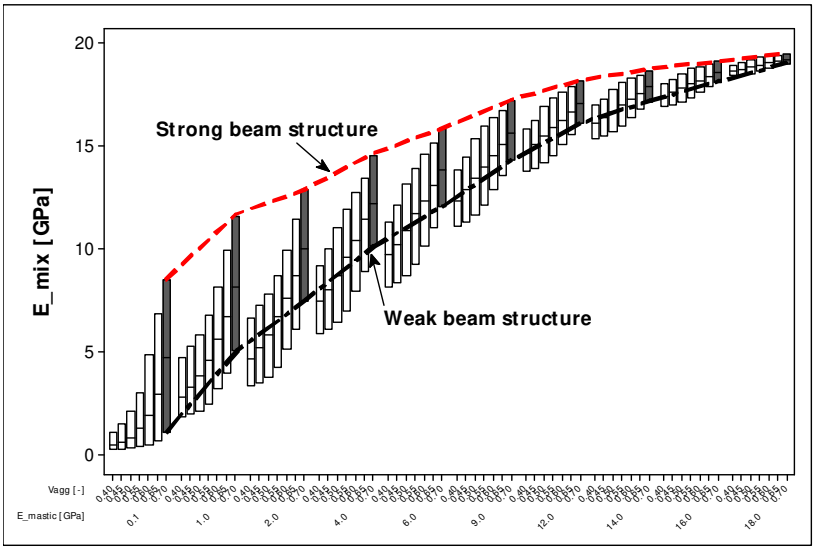

FIGURE 21 Extreme E_{mix} data points for V_{agg}=0.70

Two beam structures with V_{agg}=0.70 were selected for further analysis. They are shown in Figure 22. The stronger beam has high aggregate phase connectivity and mastic phase elements scatter over the entire beam structure. The weaker beam has several cross-sections made entirely of mastic elements.

FIGURE 22 Weak (right) and strong (left) beam structures (V_{agg}=0.70)

From the simulations, approximate relations between mixture modulus E_{mix} and mastic modulus E_{ma} were obtained. The results are shown in normalized form in Figure 23.

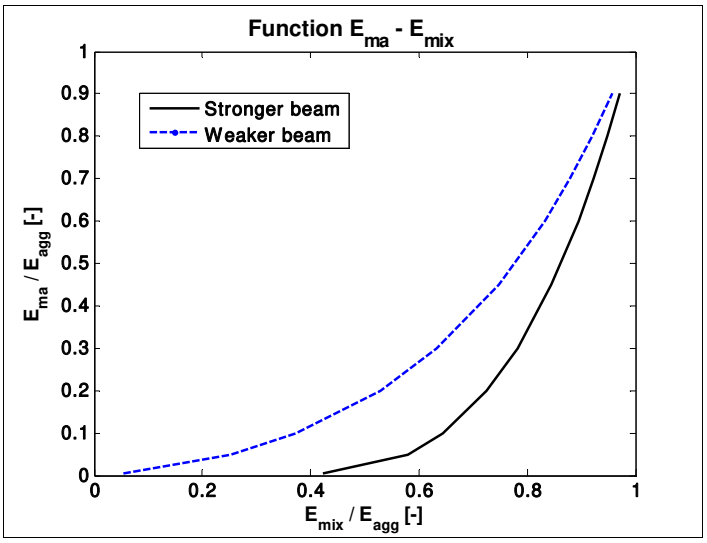

FIGURE 23 E_{ma} as a function of E_{mix} for strong and weak beam structure

Mastic creep compliance $J_{ma}(t)$ can then be calculated. The results are shown in Figure 24.

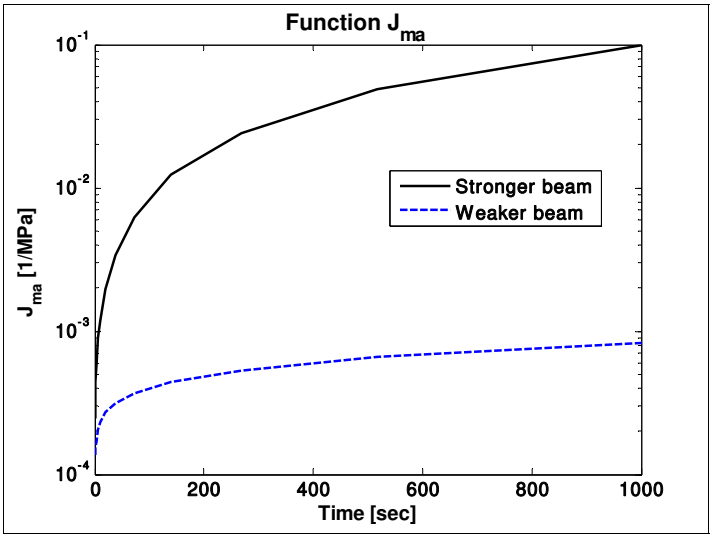

FIGURE 24 J_{ma} predictions for strong and weak beam structure

A significant difference in the $J_{ma}(t)$ predictions is observed for the two beam structures, which indicates that aggregate spatial distribution in asphalt mixtures is very important. Therefore, not only the aggregate volume fraction but also the aggregate structure within the mixture should be taken into account when using an inverse model to predict creep compliance of the mastic or binder. This information can be obtained with different methods such as X-Ray CT or 2D image scanning combined with ABAQUS FEM simulations. However, these methods are rather complex and a more practical method for obtaining mixture internal structure is needed. This issue is further addressed in the next chapter.

6.2 COMPOSITE MATERIALS MODELS

At the macroscopic level composite materials consist of two or more phases. One or more phases, called inclusion, are dispersed in a continuous matrix. In order to correctly predict the performance of the particular composite material, one needs to know not only the properties of its constituents and their volumetric proportions in the composite but also their arrangement and connectivity at the microscopic level. This higher-order microstructural information is difficult to obtain. In the literature a significant number of models are available to estimate the microstructure correlation functions of composite materials (*13*, *14*). The effective response $\boldsymbol{K_{eff}}$ of the composite can be written in a general form as:

$$\mathbf{K_{eff}} = f\left(\mathbf{K_i}, \phi_i, \boldsymbol{\Omega}\right) \quad [9]$$

where $\boldsymbol{K_i}$ and ϕ_i represent the intrinsic properties of the i^{th} phase and its volumetric fraction in the composite, respectively, and $\boldsymbol{\Omega}$ indicates the functionals of the higher-order microstructural information.

In order to model the behavior of composite materials at the microscopic level three steps are required:

- Microstructure reconstruction and phase identification.
- Determination of phase properties.
- Modeling of the effective response $\boldsymbol{K_{eff}}$.

The reconstruction of the microstructure and phase identification is not a simple task. In order to perform it, the phase volume (or area) fractions, the surface (or length) of interfaces, orientation, shape, and spatial distribution of inclusion phases must be considered. Furthermore, information on the connectivity of different phase domains is also required. Different correlation functions might be used (*14*) to estimate the above mentioned parameters; those functions may then be used as input in the effective response models. Some examples are:

- n-point probability functions $S_n^{(i)}$
- Surface correlation functions,
- Pore-size probability density function P,
- Point/q-particle correlation functions,
- Nearest-neighbor probability density function H_p.

Realization of the microstructure is one of the steps required to create the base for estimating phase volume fraction and/or correlation functions. Several options are available: Gaussian random fields (*15*) or Monte Carlo method (*14*) can be used in a computer simulation, and digital image acquisition of the existing composite material (*13*).

In the second step every realization of the composite material has to be sampled so the correlation functions can be computed from each sample. Averaging over all samples provides a good estimate of the correlation functions.

In the case of asphalt mixture analysis, 2D imaging (*16, 17, 18, 19, 20*) and X-ray computer tomography (*21, 22, 23*) are the most common reconstruction methods based on imaging technique. Further analyses are then possible after Digital Image Processing (DIP) techniques are applied (*24*). Another alternative method that has not been applied to asphalt mixtures is stereology, which allows simulating 3D structure from 2D images (*13, 25*). The intrinsic properties $\boldsymbol{K_i}$ of composite material constituents have to be known (*26*) in order to predict its effective response $\boldsymbol{K_{eff}}$.

In this research effort a number of models were investigated and are listed below.

- Voight and Reuss Bounds (laws of mixture) (*27*)
- Hashin and Shtrikman Bounds (*28*)
- Milton Improved Bounds with Miller Equations for Geometry Parameter Z_1 (*29*, *30, 31, 32, 33, 34*)
- Generalized Self-Consistent Scheme (GSCS) (*35, 36, 37, 38, 39*)
- Hirsch Model (*8, 40*)
- Self-Consistent Method (SCM) (*41, 42*)

The last four models were then applied to the experimental results from 3-point bending test. A detailed description of the models and their application to asphalt mixture creep stiffness data is presented elsewhere (*3,* Error! Reference source not found.**)**. In this report, only Hirsch model is presented in detail since the analysis indicated that it represented the best predicting model, and was further used in the backcalculation procedure described in the next chapter.

6.2.1 Hirsch Model

Several mechanical models based on Hirsch model (*8*) were reviewed by *Christensen et al.* (*40*) and a three phase semi-empirical mechanical model, consisting of aggregates, asphalt binder and air voids set in a parallel and in series arrangements, was proposed for extensional $|E^*|_{mix}$ and shear $|G^*|_{mix}$ dynamic modulus of the asphalt mixture. The model is shown in Figure 25.

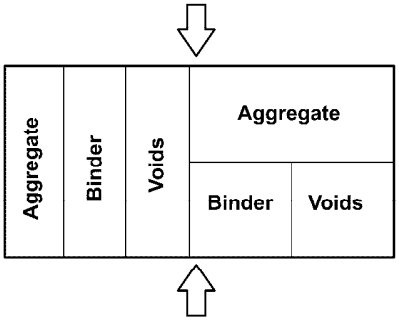

FIGURE 25 Semi-empirical model proposed by *Christensen et al. (44)*

The model's general equation is given by the following equation:

$$E_{mix} = Pc\left[E_{agg}V_{agg} + E_{binder}V_{binder}\right] + \left(1 - Pc\right)\left[\frac{V_{agg}}{E_{agg}} + \frac{\left(1 - V_{agg}\right)^2}{E_{binder}V_{binder}}\right]^{-1} \quad [10]$$

The parameter *contact volume Pc* takes into account the relative proportions of the series and parallel phases and has the following expression:

$$Pc = \frac{\left(P_0 + \frac{VFA \cdot E_{binder}}{VMA}\right)^{P1}}{P_2 + \left(\frac{VFA \cdot E_{binder}}{VMA}\right)^{P1}} \quad [11]$$

where

VMA = voids in mineral aggregate [%], $VMA=100-V_{agg,}$

VFA = voids filled with binder [%], $V_{binder}=VFA*VMA$.

E_{binder} = stiffness of the asphalt binder used in the mix

P_0, P_1, P_2 = fitting parameters.

The model described by equation [10] was applied to the experimental data used in this research. Since the model (as well as the models not described here) is expressed in terms of modulus rather than compliance, the experimental creep data was converted to relaxation modulus using Hopkins and Hamming numerical method (44).

Two different expressions were used for *Pc*: equation [11] and an alternative expression:

$$Pc = a\ln\left(E_{binder}\right) + b \quad [12]$$

The original *Pc* was calculated based on the VMA and VFA of mixtures in the range of 13.7 to 21.6% and 38.7 to 68.0%, respectively. Since the mixtures used in this research were produced using very similar mix designs, the volumetric information was removed from *Pc* expression to obtain a simpler form.

Figure 26 shows the predicted and measured modulus values using both expressions for *Pc*. It was found that E_{mix} values for both aggregate types were consistently over predicted by the original Hirsch model, as shown in the left hand plot. It is hypothesized that the different mode of loading used to calibrate the original Hirsch model is responsible for this difference. The right hand plot shows that Hirsch model with the new expression for *Pc* is able to predict the measured E_{mix} relatively well for both aggregate types used (granite and limestone) and all points seem to follow the line-of-equality (LOE).

The coefficients of Equation 14 were calculated as: 0.100 and 0.609 and provide the following expression for *Pc*:

$$Pc = 0.100 \cdot \ln\left(E_{binder}\right) + 0.609 \quad [13]$$

where E_{binder} is expressed in GPa.

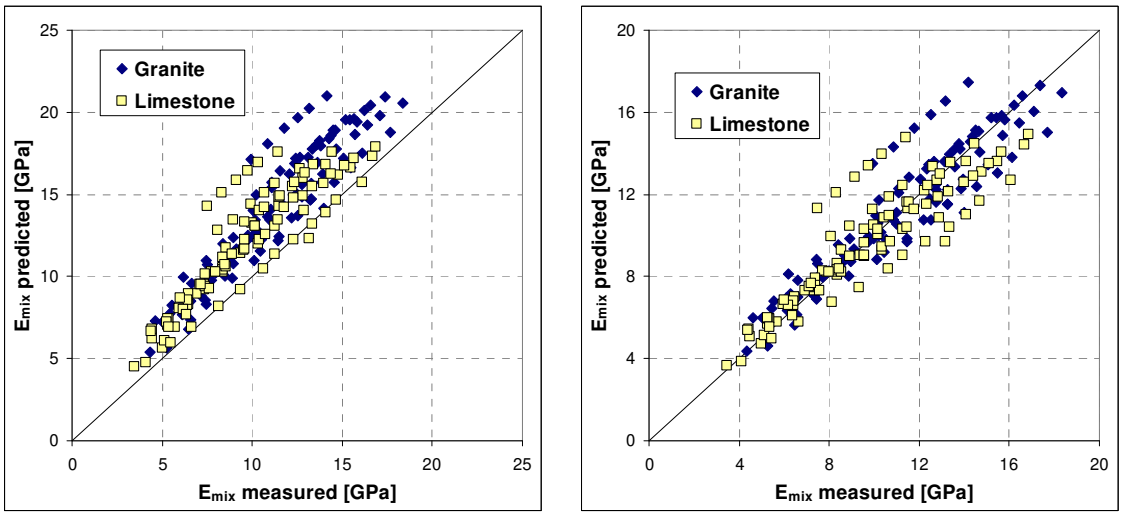

FIGURE 26 Hirsch model predictions using, a) original *Pc*, b) proposed *Pc*

The $E_{mix}(t)$ predictions using equation [15] to calculate *Pc* for a PG 58-34 GR M2 mixture at two test temperatures are shown in Figure 27 . The predicted values match the experimental data very well.

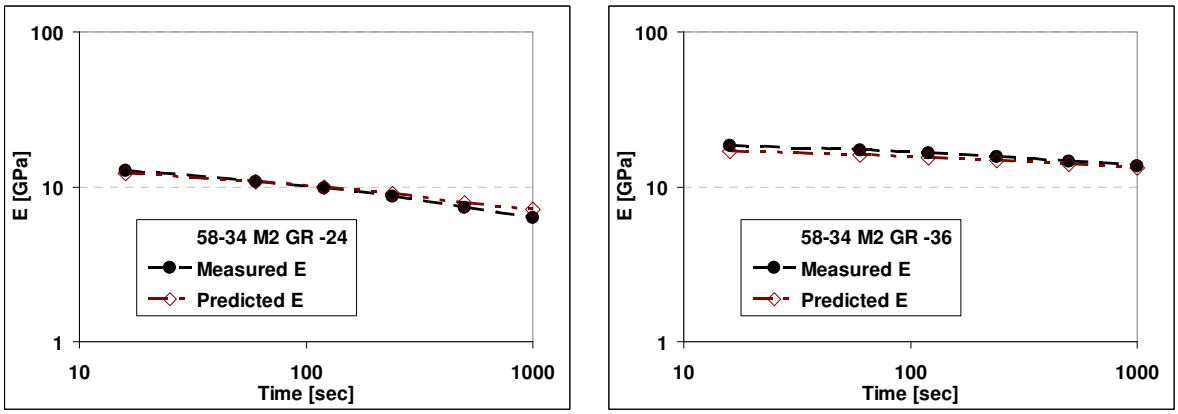

FIGURE 27 Hirsch model predictions with proposed *Pc*, a) -24°C, b) -36°C

6.3 CONCLUSIONS

The Finite Element simulations for a homogeneous asphalt mixture indicate that IDT and BBR produce similar results, within 4% of each other. This is similar to the results obtained from the analysis of the polymeric materials experimental data. Additional simulations performed to evaluate the effect of aggregate structure indicates that aggregate spatial distribution in asphalt mixtures is very important and therefore, not only the aggregate volume fraction but also the aggregate structure within the mixture should be taken into account when using an inverse model to predict the properties of the mixture components. This information can be obtained with different methods such as X-Ray CT or 2D image scanning combined with ABAQUS FEM simulations.

A number of micromechanics models were also evaluated. It was found that modified Hirsch model is the most promising predictive model and its use in backcalculating the binder properties is further evaluated in the next chapter.

CHAPTER 7

BACK-CALCULATION OF ASPHALT BINDER CREEP COMPLIANCE

In section 6.2, four micromechanics models were evaluated in terms of their ability to predict asphalt mixture low temperature properties and to bakcalculate mixture components properties. The analyses performed indicated that *SCM* model does not work for the considered dataset and that both *Milton* and GSCS models require additional adjustment factors, which introduce more error into the potential inverse schemes. Moreover, the expressions for *Milton* and GSCS models are complicated and E_{binder} cannot be explicitly derived from them.

A simple backcalculation scheme based on Hirsch model was developed by *Zofka et al. (3, 0*) for the case when the mixture volumetrics information (VMA and VFA) is known. The idea came from the observation that at low temperatures, the shape of the mix stiffness function predicted using Hirsch model is very simple and most likely could be fitted using a much simpler expression. The approach consists of the following steps:

- First, a plot of S_{mix} as a function of S_{binder} is generated using equation [10] in which E_{mix} and E_{binder} are replaced by S_{mix} and S_{binder}, respectively. P_c is calculated using equation [13]. The plot is generated by inputting the known mixture volumetric properties and assuming equally-spaced S_{binder} values from 10MPa to 2.0GPa, as shown in Figure 28.

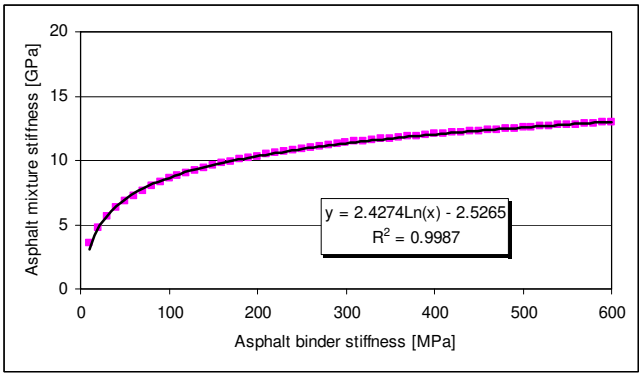

FIGURE 28 Simplified mixture stiffness function

- The generated function is then refitted with a much simpler expression:
  $S_{mix} = a_1 * \ln(S_{binder}) + b_1$ [16]
  from which a_1 and b_1 are calculated for the given asphalt mixture
- S_{binder} is simply calculated by solving the linear equation in terms of $\ln(S_{binder})$.

Preliminary use of this approach (*0*) indicated excellent agreement in some cases, as shown in Figure 29.

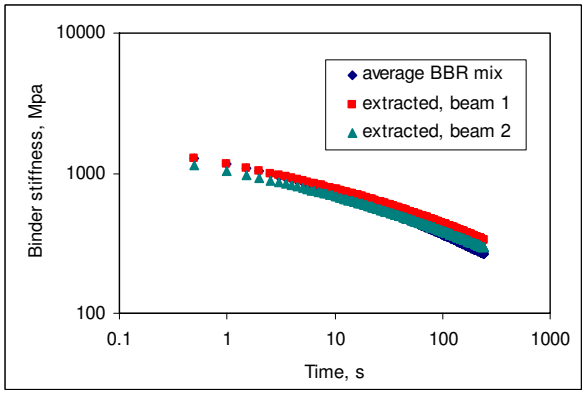

FIGURE 29 Comparison of experimentally obtained and back-calculated stiffness curves at -24ºC.

This approach was used with the data generated as part of this investigation. For all mixtures tested, the Hirsch model predicted S_{mix} could be fitted very well with a very simple linear function of $\ln(S_{binder})$. Examples for two of the mixtures tested are shown in Figure 30.

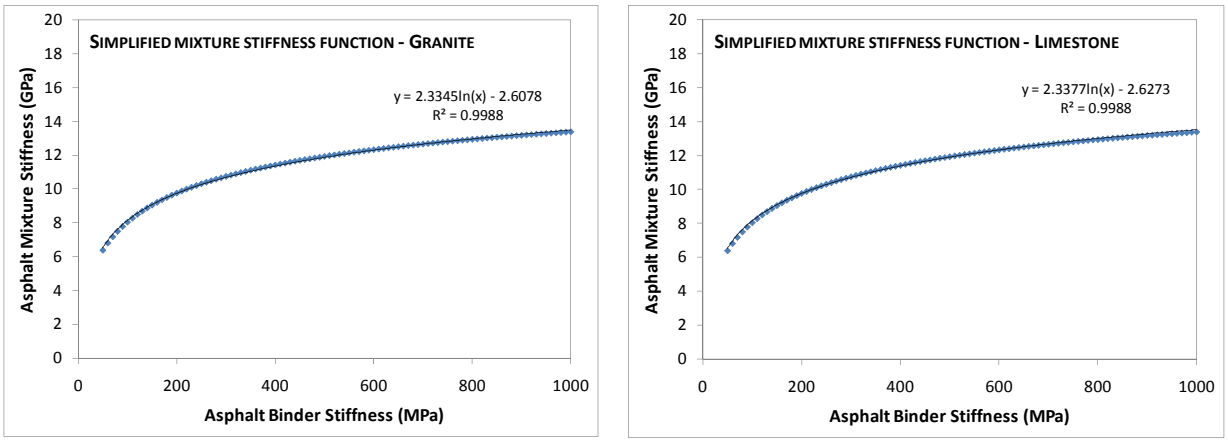

FIGURE 30 Simplified mixture stiffness function (Granite and Limestone)

The backcalculation algorithm was then applied to the mixture data and binder creep stiffness data was obtained and compared to the creep stiffness experimentally determined for the RTFOT binders used to prepare the corresponding mixtures. The comparison of the predicted and experimentally determined data indicated less good agreement than the results previously reported (*0*). It should be mentioned that in this previous work, the binders were chemically extracted from the mixture and then tested, while in the current work the original binder was aged in the RTFOT and then tested. Examples are shown in Figure 31.

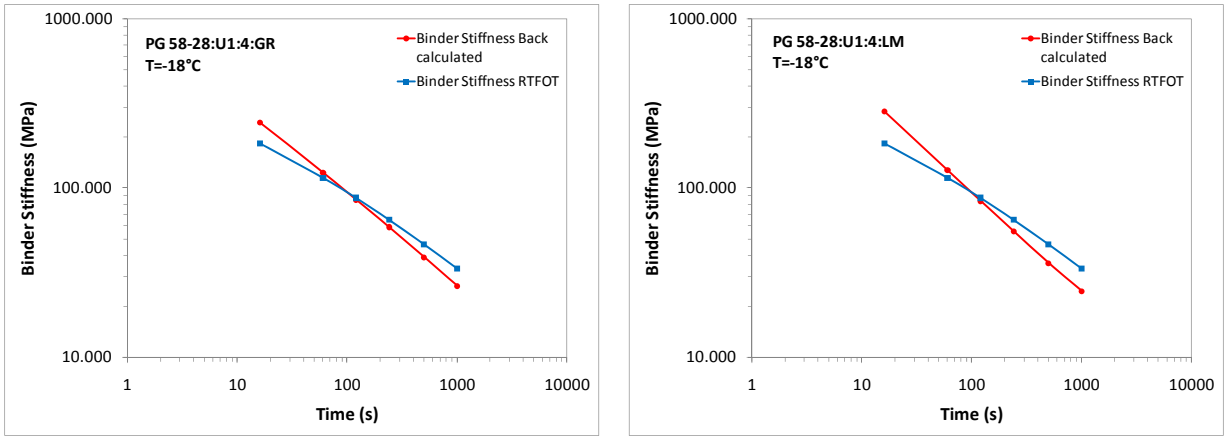

FIGURE 31 Comparison of experimental and back-calculated creep stiffness, PG 58-28:U1 at -18ºC.

These results suggest that further investigation is required to obtain a robust backcalculation algorithm. It is anticipated that the improved method will require additional information about the aggregate spatial distribution in asphalt mixtures, which can be obtained using various digital imaging techniques, as described in the previous chapter.

This approach can also provide volumetrics information in situations where the mix design is not available. Preliminary work performed at University of Minnesota indicated that image processing of scanned BBR mixture specimens can be used to obtain reasonable estimates of VMA and VFA. The biggest obstacle in obtaining highly accurate values is identifying the correct amount of filler (particles smaller than 75microns) used, which cannot be determined through digital imaging. An example is shown in the next table, in which information from scanned images of BBR beams and assumptions of volume ratio of aggregates larger than 75 microns to aggregates smaller than 75 microns were used to obtain the VMA of an asphalt mixture. The VMA calculated from standard laboratory measurements was 24.

TABLE 11 Corrected Values of VMA for Different Volume Ratios of Aggregates

VMA uncorrected (%)	VMA corrected (%)		
	Volume Ratio = 3	Volume Ratio = 7	Volume Ratio = 19
34.15	12.20	24.74	30.68

The most promising application of this method is for mixtures prepared with various amounts of RAP. The backcalculation procedure can be used to predict the binder properties in the mix, which may provide a reasonable indicator of how much blending occurs between the aged binder and the new binder. This information can be used to perfect the mix design as well as the plant fabrication process in terms of RAP gradation, plant temperature, and mixing time.

CHAPTER 8

CONCLUSIONS, PLANS FOR IMPLEMENTATION, AND RECOMMENDATIONS FOR FURTHER RESEARCH

8.1. CONCLUSIONS

The idea of performing creep tests on asphalt mixture beam specimens with the Bending Beam Rheometer (BBR) was investigated in this project. The BBR testing procedure has many advantages over the current IDT specification such as: most if not all asphalt testing laboratories have the BRR; the price is reasonable; BBR has very good performance and reliability; the calibration verification is very simple. In addition, the smaller size specimen makes possible investigating the properties of thin layers of asphalt mixtures at different depths in the pavement.

In the first part of the investigation a detailed beam preparation procedure was developed for both laboratory compacted and field cores. Based on the measurements collected for 660 thin beams, it was found that uniform BBR mixture beams can be produced. The average coefficient of variation for the thickness and width of individual beams, based on measurements at three locations along the length of the beam, were 2.12% and 1.23%, respectively. Measured thickness ranged from 5.31 to 6.57 mm with a 2.43% coefficient of variation. Measured width varied from 12.02 to 12.90 mm, with a coefficient of variation of 0.98%. For accurate results, the beams need to be measured before the one hour isothermal storage and the correct beam thickness and width need to be input in the test software.

A detailed loading procedure was developed next. It was determined that good results can be obtained using the current BBR device and test loads of 1961 mN and 4413 mN at (PG low temperature + 22˚C) and (PG low temperature + 10˚C) respectively. At (PG low temperature - 2˚C), it is recommended to predict the creep stiffness from the data obtained at the higher two temperatures and from time-temperature superposition. Based on the tests performed, it was found that the cooling medium and reasonable variations in air voids do not significantly affect asphalt mixture creep stiffness results at low temperature.

One of the main objectives of this investigation was to determine if BBR experimental results match the IDT results. Experimental data obtained for 20 laboratory mixtures that consist of combinations of aggregate type, binder type, air voids, and asphalt content and field cores from 4 pavements were used in the analysis. For asphalt mixtures, a simple linear relationship was obtained between the IDT creep stiffness and the BBR creep stiffness obtained at (PG low temperature + 22˚C) and (PG low temperature + 10˚C): IDT creep stiffness was approximately equal to 86.5% of the BBR creep stiffness. The IDT experimental data at (PG low temperature - 2˚C) was not always reliable, due to the formation of ice around extensometers and very small deformations, and was not included in the analysis. A similar relation could not be identified for the field samples, most likely due to the aging gradient in field cores. For the two polymeric materials tested, differences of less than 3% were observed between IDT creep stiffness and BBR creep stiffness. This appears to indicate that a portion of the difference between the BBR and IDT data can be explained by the non-homogeneous nature of asphalt mixtures.

To further address the concern that small BBR specimens may not be representative of the asphalt pavement, the critical issue of the representative volume element (RVE) was investigated by performing three-point bending creep tests on beams of three different sizes. The statistical analysis of the 1x, 2x and 3x beams experimental data indicated that BBR asphalt mixture beams (1x) are an RVE of the material for (PG low limit + 22˚C) and (PG low limit + 10˚C). At the lowest test temperature (PG low limit - 2˚C), a robust analysis could not be performed due to the variability of the results due to the difficulties associated with testing the 2x and 3x beams.

The influence of specimen geometry (IDT vs. BBR) and of the aggregate spatial distribution in the BBR beam was investigated by means of finite element modeling. The Finite Element simulations for a homogeneous asphalt mixture produced similar results for IDT and BBR, within 4% of each other, similar to the experimental results for two polymeric materials. Additional simulations performed to evaluate the effect of aggregate structure indicated that aggregate spatial distribution in asphalt mixtures is very important and therefore, not only the aggregate volume fraction but also the aggregate structure within the mixture should be taken into account when using an inverse model to predict the properties of the mixture components.

A number of micromechanics models were also evaluated. Selection of an accurate micromechanics model is critical in estimating the contribution of the component phases of a composite material and in developing backcalculating algorithms to estimate these contributions from tests performed on the composite material. It was found that the modified Hirsch model is the most promising predictive model and its use in backcalculating the binder properties was further

analyzed. A simple algorithm, previously developed, was applied to the experimental data obtained in this research. The results although reasonable, indicated that further investigation was needed to better predict the component asphalt binder creep stiffness from mixture testing. This would require information about aggregate spatial distribution in asphalt mixtures and knowledge about volume ratio of aggregates larger than 75 microns to aggregates smaller than 75 microns

8.2. PLANS FOR IMPLEMENTATION

The research performed in this project was presented at national and international meetings and has received considerable attention over the past year. Minnesota Department of Transportation and Utah Department of Transportation have already expressed their interest in implementing the test method as part of routine testing. Based on input from panel members and the asphalt community, a draft specification for obtaining low temperature creep stiffness of asphalt mixtures using the BBR was developed and will be presented at the next Asphalt Mixture ETG meeting in September for further comments. It is anticipated that, with support from Georgia Department of Transportation Materials and Research Engineer, and Minnesota Department of Transportation and Utah Department of Transportation Asphalt Engineers, a draft specification (see Appendix A; note that precision and bias values are not available at this time) will be submitted to AASHTO by the end of the year.

8.3. RECOMMENDATIONS FOR FURTHER RESEARCH

The results obtained in this investigation indicated the need for more extensive research to develop micromechanics models that can be used to accurately backcalculate asphalt binder creep stiffness from mixture testing. Preliminary work performed at University of Minnesota suggests that using digital imaging techniques with scanned images of BBR asphalt mixture beams can provide particle size distribution and volumetric fraction information required by a rigorous backcalculation procedure. This approach has also the potential to become a simple “fingerprint” tool for quality control and can be used to provide information about distribution of RAP particles in new mixtures and improve RAP processing methods.

Based on feedback from paper and poster presentations at TRB, AAPT, and ETG discussions, additional research is needed to further improve the BBR method to obtain asphalt mixture strength as well, similar to the current IDT procedure. Both the creep stiffness and strength are needed in the AASHTO Mechanistic Empirical Pavement Design Guide low temperature algorithm (TC Model) to predict low temperature performance. This requires a system with a heavier loading frame and the capability of applying a constant loading rate from zero to failure. Cannon Industries has already delivered to University of Minnesota a heavier loading system and will deliver in the near future a proportional valve control component that allows loading at constant loading rate. The new system will be capable of performing both creep and strength tests on thin mixture beams and on asphalt binder beams.

REFERENCES

1. American Association of State Highway and Transportation Officials (AASHTO) Standard T313-08, "Standard method of test for determining the flexural creep stiffness of asphalt binder using the Bending Beam Rheometer (BBR)", Standard Specifications for Transportation Materials and Methods of Sampling and Testing, 2009 Edition.
2. American Association of State Highway and Transportation Officials (AASHTO) Standard T 322-07. "Determining the Creep Compliance and Strength of Hot-Mix Asphalt (HMA) Using the Indirect Tensile Test Device". Standard Specifications for Transportation and Methods of Sampling and Testing, 2009 Edition.
3. A. Zofka. Investigation of Asphalt Concrete Creep Behavior Using 3-Point Bending Test. PhD thesis, University of Minnesota, Minneapolis, July 2007.
4. M. Marasteanu, A. Zofka, M. Turos, X. Li, R. Velasquez, X. Li, W. Buttlar, G. Paulino, A. Braham, E. Dave, J. Ojo, H. Bahia, C. Williams, J. Bausano, A. Kvasnak, A. Gallistel, J. McGraw, *Investigation of Low Temperature Cracking in Asphalt Pavements National Pooled Fund Study 776 Final Report*. October 2007. Prepared for: Minnesota Department of Transportation Research Services MS 330.
5. M. Marasteanu. The Role of Bending Beam Rheometer Parameters in Thermal Stress Calculations. Transportation Research Record No. 1875, 2004, pp. 9-13.
6. American Association of State Highway and Transportation Officials (AASHTO) Designation T166-05: "Bulk Specific Gravity of Compacted Asphalt Mixtures Using Saturated Surface-Dry Specimens". Standard Specifications for Transportation Materials and Methods of Sampling and Testing, 26th Edition, Washington D.C., 2006.
7. American Association of State Highway and Transportation Officials (AASHTO) Designation T209-05: "Theoretical Maximum Specific Gravity and Density of Bituminous Paving Mixtures". Standard Specifications for Transportation Materials and Methods of Sampling and Testing, 26th Edition, Washington, D.C., 2006.
8. T. J. Hirsch. Modulus of elasticity of concrete affected by elastic moduli of cement paste` matrix and aggregate. Journal of the American Concrete Institute vol. 59(3), 1962, pp. 427-452
9. R. Roque, W. Buttlar. The development of a measurement and analysis system to accurately determine asphalt concrete properties using the Indirect Tensile mode. Journal of the Association of Asphalt Paving Technologists, vol. 61, 1992, pp. 304-328
10. M. Frocht. *Photoelasticity*. vol. II, John Wiley & Sons Inc., New York, 1948
11. W. Buttlar, R. Roque. Development and evaluation of the Strategic Highway Reasearch Program measurement and analysis system for Indirect tensile testing at low temperatures. Transportation Research Record, vol. 1454, 1994, pp. 163-171
12. J. Gere, S. P. Timoshenko. *Mechanics of materials*. PWS-KENT Publishing Company, Boston, 3rd edition, 1990
13. E. J. Garboczi, D. P. Bentz, N. S. Martys. Digital images and computer modelling. Experimental Methods in the Physical Sciences, vol. 35, 1999, pp. 1-41
14. S. Torquato. *Random heterogeneous materials*. Springer-Verlag, New York, 2002
15. S. Hayasaka, T. E. Nichols. Validating cluster size inference: random field and permutation methods. NeuroImage, vol. 20 2003, pp. 2343–2356
16. A. R. Abbas, A. T. Papagiannakis, E. A. Masad. Linear and nonlinear viscoelastic analysis of the microstructure of asphalt concretes. Journal of Materials in Civil Engineering, vol. 16(2), 2004, pp. 133-139
17. E. Masad, N. Somadevan. Microstructural Finite-Element analysis of influence of localized strain distribution on asphalt mix properties. Journal of Engineering Mechanics, vol. 128(10), 2002, pp. 1105-1114
18. A. T. Papagiannakis, A. Abbas, E. Masad. Micromechanical analysis of viscoelastic properties of asphalt concretes. Journal of the Transportation Research Board, vol. 1789, 2002, pp. 113-120
19. Z. You, W. Buttlar. Discrete Element Modeling to predict the modulus of asphalt concrete mixtures. Journal of Materials in Civil Engineering, vol. 16(2), 2004, pp. 140-146
20. Z. Q. Yue, S. Chen, L. G. Tham. Finite element modeling of geomaterials using digital image processing. Computers and Geotechnics, vol. 30, 2003, pp.375-397.
21. E. Masad, V. K. Jandhyala, N. Dasgupta, N. Somadevan, N. Shashidhar. Characterization of air void distribution in asphalt mixes using X-ray Computed Tomography. Journal of Materials in Civil Engineering, vol. 14(2), 2002, pp. 122-129.
22. L. B. Wang, J. D. Frost, N. Shashidhar. Microstructure study of WesTrack mixes from X-ray tomography images. Journal of the Transportation Research Board, vol. 1767, 2001, pp. 85-94
23. L. B. Wang, X. Wang, L. Mohammad, Y. Wang. Application of mixture theory in the evaluation of mechanical properties of asphalt concrete. Journal of Materials in Civil Engineering, vol. 16(2), 2004, pp. 167-174.

24. R. C. Gonzalez, R. E. Woods, S. L. Eddins. *Digital image processing*. Upper Saddle River, Pearson Prentice Hall, 2004
25. C. L. Y. Yeong, S. Torquato. Reconstructing random media. Physical Review E, vol. 57(1), 1998, pp. 495-506
26. M. D. Isaac, O. Ishai. Engineering *mechanics of composite materials*. Oxford University Press, New York, 2006
27. S. Torquato. Modeling of physical properties of composite materials. International Journal of Solids and Structures, vol. 37, 2000, pp. 411-422
28. Z Hashin. Analysis of composite materials – a survey. Journal of Applied Mechanics, vol. 50, 1983, pp. 481-505
29. G. W. Milton. Bounds on the electromagnetic, elastic, and other properties of two-component composites. Physical Review Letters, vol. 46(8), 1981, pp. 542-545
30. S. Torquato. Random heterogeneous media: microstructure and improved bounds on effective properties. Applied Mechanics Review, vol. 44(2), 1991, pp. 37-76
31. J. G. Berryman. Variational bounds on elastic constants for the penetrable sphere model. Journal of Physics. D: Applied Physics, vol. 18, 1985, pp. 585-597
32. J. G. Berryman, G. W. Milton. Microgeometry of random composites and porous media. Journal of Physics. D: Applied Physics, vol. 21, 1988, pp. 87-94
33. J. G. Berryman. Measures of microstructure to improve estimates and bounds on elastic constants and transport coefficients in heterogeneous media. Mechanics of Materials, vol. 38, 2006, pp. 732-747
34. M. N. Miller. Bounds for effective electrical, thermal, and magnetic properties of heterogeneous materials. Journal of Mathematical Physics, vol. 10(11), 1969, pp. 1988-2004
35. R. M. Christensen. *Mechanics of composite materials*. Dover Publications, INC., Mineola, New York, 1979
36. R. M. Christensen, K. H. Lo. Solutions for effective shear properties in three phase sphere and cylinder models. Journal of the Mechanics and Physics of Solids, vol. 27, 1979, pp. 315-330
37. Z. Hashin. Viscoelastic behavior of heterogeneous media. Journal of Applied Mechanics, vol. 9, 1965, pp. 630-636
38. W. Buttlar, D. Bozkurt, G. G. Al-Khateeb, A. S. Waldhoff. Understanding asphalt mastic behavior through micromechanics. Transportation Research Record, vol. 1681, 1999, pp.157-166
39. N. Shashidhar, A. Shenoy. On using micromechanical models to describe dynamic mechanical behavior of asphalt mastics. Mechanics of Materials, vol. 34, 2002, pp. 657-669
40. D. Christensen, T. Pellinen, R. F. Bonaquist. Hirsch model for estimating the modulus of asphalt concrete. Journal of Association of Asphalt Paving Technologists, vol. 72, 2003, pp. 97-121
41. R. Hill. A self-consistent mechanics of composite materials. Journal of the Mechanics and Physics of Solids, vol. 13, 1965, pp. 213-222
42. H. M. Yin, W. Buttlar, G. Paulino, H. Di Benedetto. Micromechanics-based model for asphalt mastics considering viscoelastic effects. 10th International Conference on Asphalt Pavements, August 12-17 2006, Quebec City, Canada
43. R. A. Velasquez. On the Representative Volume Element of Asphalt Concrete. PhD Thesis, University of Minnesota, Minneapolis, June 2009.
44. I. L. Hopkins, R. W. Hamming. On creep and relaxation. Journal of Applied Physics, vol. 28, 1957, pp. 906-909
A. Zofka, M. Marasteanu, X. Li, T. Clyne, J. McGraw. Simple method to obtain asphalt binders low temperature properties from asphalt mixtures properties. Journal of the Association of Asphalt Paving Technologists, vol. 80, 2005, pp.255-282.

Standard Method of Test for

Determining the Flexural Creep Stiffness of Asphalt Mixtures Using the Bending Beam Rheometer (BBR)

AASHTO Designation: T xxx-xx

PROVIDED AS AN EXAMPLE ONLY - NOT FOR DISTRIBUTION

Standard Method of Test for

Determining the Flexural Creep Stiffness of Asphalt Mixtures Using the Bending Beam Rheometer (BBR)

AASHTO Designation: T xxx-xx

1. SCOPE

1.1. This test method covers the determination of the flexural creep stiffness or compliance of asphalt mixtures by means of a bending beam rheometer. It is applicable to material having a flexural stiffness value from 20 MPa to 20 GPa (creep compliance values in the range of 50 nPa–1 to 0.05 nPa–1). The test apparatus is designed for testing within the temperature range from –36 to 0°C.

1.2. Test results are not valid for beams of asphalt mixtures that deflect more than 300μm (5% of beam thickness), or less than 30 μm, when tested in accordance with this method.

1.3. *This standard may involve hazardous materials, operations, and equipment. This standard does not purport to address all of the safety concerns associated with its use. It is the responsibility of the user of this procedure to establish appropriate safety and health practices and to determine the applicability of regulatory limitations prior to use.*

2. REFERENCED DOCUMENTS

2.1. *AASHTO Standards*:

- M 320, Performance-Graded Asphalt Binder
- R 28, Accelerated Aging of Asphalt Binder Using a Pressurized Aging Vessel (PAV)
- T 40, Sampling Bituminous Materials
- T 240, Effect of Heat and Air on a Moving Film of Asphalt Binder (Rolling Thin-Film Oven Test)
- T 312, Preparing and Determining the Density of Hot Mix Asphalt (HMA) Specimens by Means of the Superpave Gyratory Compactor

2.2. *ASTM Standards*:

- C 670, Practice for Preparing Precision and Bias Statements for Test Methods for Construction Materials
- C 802, Conducting an Interlaboratory Test Program to Determine the Precision of Test Methods for Construction Materials
- E 77, Standard Test Method for Inspection and Verification of Liquid-in-Glass Thermometers
- E 220, Method for Calibration of Thermocouples by Comparison Techniques

2.3. *Deutche Industrie Norm (DIN) Standards*:

- 43760, Platinum Resistance Thermometer

3. TERMINOLOGY

3.1. *Definitions*:

3.1.1. *asphalt mixtures*—an asphalt-based composite material that consists of asphalt cement, coarse and fine aggregates, filler, and air voids.

3.1.2. *physical hardening*—a time-dependent stiffening of asphalt mixtures that results from the time-delayed increase in stiffness when the asphalt mixtures are stored at low temperatures. The increase in stiffness due to physical hardening is reversible when the temperature is raised.

3.2. *Descriptions of Terms Specific to This Standard*:

3.2.1. *flexural creep*—a test in which a simply-supported asphalt mixures prismatic beam is loaded with a constant load at its midpoint and the deflection of the beam is measured with respect to loading time.

3.2.2. *measured flexural creep stiffness,* $S_m(t)$—ratio obtained by dividing the maximum bending stress in the beam by the maximum bending strain.

3.2.3. *estimated creep stiffness,* $S(t)$—the creep stiffness obtained by fitting a second order polynomial to the logarithm of the measured stiffness at 8.0, 15.0, 30.0, 60.0, 120.0, 240.0, and the logarithm of time.

3.2.4. *flexural creep compliance,* $D(t)$—ratio obtained by dividing the maximum bending strain in the beam by maximum bending stress. $D(t)$ is the inverse of $S(t)$. $S(t)$ has been used historically in asphalt technology while $D(t)$ is commonly used in studies of viscoelasticity.

3.2.5. *m-value*—absolute value of the slope of the logarithm of the stiffness curves versus the logarithm of the time.

3.2.6. *contact load*—load required to maintain positive contact between the beam and the loading shaft; 35 ±10 mN.

3.2.7. *seating load*—load of 1-s duration required to seat the beam; 1961 ±50 mN and 4413 ±50 mN for high and for intermediate temperature levels respectively (high temperature level = low temperature grade of binder + 10˚C + 12˚C; intermediate temperature level = low temperature grade of binder + 10˚C).

3.2.8. *test load*—load of 240-s duration required to determine the stiffness of material being tested; 1961 ±50 mN and 4413 ±50 mN for high and for intermediate temperature levels, respectively.

3.2.9. *testing zero time, s*—time at which the signal is sent to the solenoid valve to switch from zero load regulator (contact load) to the testing load regulator (test load).

3.2.9. *Hot Mix Asphalt (HMA)*—A mixture of aggregate and asphalt binder produced from an HMA plant

4. SUMMARY OF TEST METHOD

4.1. The bending beam rheometer measures the mid-point deflection of a simply supported beam of asphalt mixtures subjected to a constant load applied to the mid-point of the beam. The device operates only in the loading mode; recovery measurements are not obtained.

4.2. A test beam is placed in the controlled temperature fluid bath and loaded with a constant load for 1000s. The test load (1961 ±50 mN or 4413 ±50 mN) and the midpoint of deflection of the beam are monitored versus time using a computerized data acquisition system.

4.3. The maximum bending stress at the midpoint of the beam is calculated from the dimensions of the beam, the span length, and the load applied to the beam for loading times of 8, 15, 30, 60, 120, and 240 seconds. The maximum bending strain in the beam is calculated for the same loading times from the dimensions of the beam and the deflection of the beam. The stiffness of the beam for the loading times specified above is calculated by dividing the maximum stress by the maximum strain.

4.4. The load and deflection at 0.0 and 0.5 s are reported to verify that the full-testing load (1961 ±50 mN or 4413 ±50 mN) during the test is applied within the first 0.5 s. They are not used in the calculation of stiffness and *m*-value and should not be considered to represent material properties. The rise time of the load (time to apply full load) can be affected by improper operation of the pressure regulators, improper air bearing pressure, malfunctioning air bearing (friction), and other factors. By reporting the 0.0 and the 0.5 s signals, the user of the test results can determine the conditions of the loading.

5. SIGNIFICANCE AND USE

5.1. The test temperature for this test is related to the temperature experienced by the pavement in the geographical area for which the asphalt binder is intended.

5.2. The flexural creep stiffness or flexural creep compliance, determined from this test, describes the low-temperature, stress-strain-time response of asphalt mixtures at the test temperature within the linear viscoelastic response range.

5.3. The low-temperature thermal cracking performance of paving mixtures is related to the creep stiffness and the slope of the logarithm of the creep stiffness versus the logarithm of the time curve of the asphalt mixture.

5.4. The creep stiffness and the slope of the logarithm of the stiffness versus the logarithm of the time curve are used as performance-based specification criteria for asphalt binders in accordance with M 320.

6. APPARATUS

6.1. *Bending Beam Rheometer (BBR) Test System*—A bending beam rheometer (BBR) test system consisting of (1) a loading frame which permits the test beam, supports, and the lower part of the test frame to be submerged in a constant temperature fluid bath. (2) a controlled temperature liquid bath which maintains the test beam at the test temperature and provides a buoyant force to counterbalance the force resulting from the mass of the beam, and (3) a computer-controlled automated data acquisition component, (4) specimen molds, and (5) items needed to calibrate and/or verify the BBR.

6.1.1. *Loading Frame*—A frame consisting of a set of sample supports, a blunt-nosed shaft that applies

The load to the midpoint of the test specimen, a load cell mounted on the loading shaft, a means for zeroing the load on the test specimen, a means for applying a constant load to the loading shaft, and a deflection measuring transducer attached to the loading shaft. A schematic of the device is shown in Figure 1.

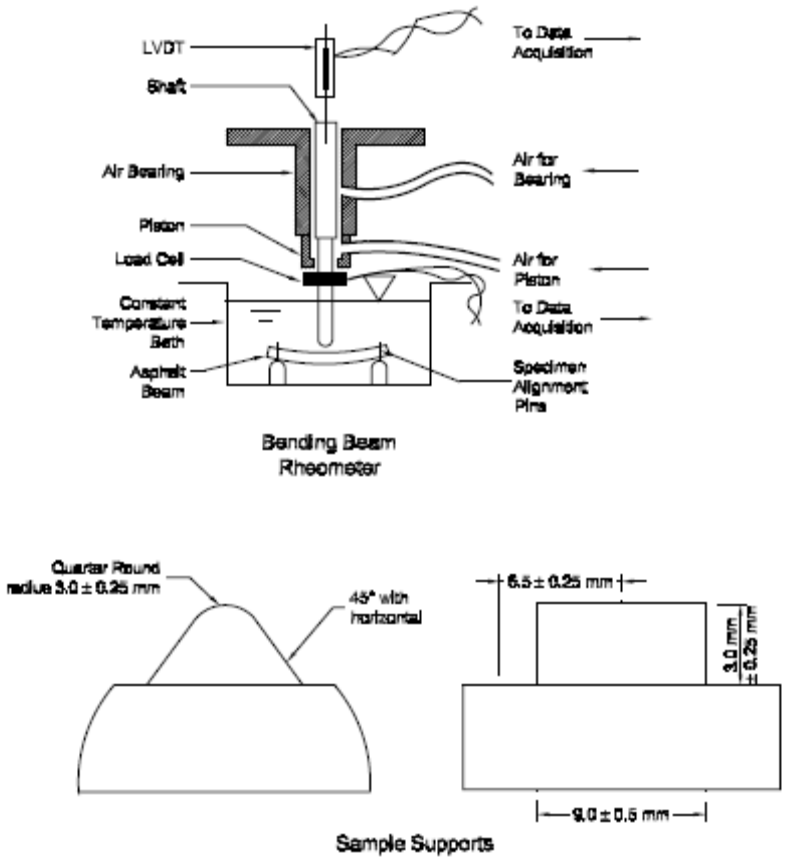

Figure 1—Schematic of the Bending Beam Rheometer

6.1.1.1. *Loading System*—A loading system that is capable of applying a contact load of 35 ± 10 mN to the test specimen and maintaining a test load of 1961 ±50 mN and 4413 ±50 mN for high and for intermediate temperature levels, respectively.

6.1.1.2. *Loading System Requirements*—The rise time for the test load shall be less than 0.5 s. The rise time is the time required for the load to rise from the 35 ±10 mN contact load to the 1961 ±50 mN and 4413 ±50 mN test load for high and for intermediate temperature levels respectively. During the rise time, the system shall dampen the test load to 1961 ±50 mN or 4413 ±50 mN. Between 0.5 and 5.0 s, the test load shall be within ±50 mN of the average test load, and thereafter shall be within ±10 mN of the average test load.

6.1.1.3. *Sample Supports*—Sample supports with specimen support strips 3.0 ±0.30 mm in top radius

and inclined at an angle of 45 degrees with the horizontal (see Figure 1). The supports, made of stainless steel (or other corrosion resistant metal), are spaced 102.0 ±1.0 mm apart. The width of the supporting area of the supporting strips shall be 9.5 ±0.25 mm. This is required to ensure that the edges of the specimen, resulting from the molding procedure, do not interfere with the mid-span deflection of the specimen measured during testing. The supports shall also include vertical alignment pins 2 to 4 mm in diameter placed at the back of each sample supports at 6.75 ±0.25 mm from the center of the supports. These pins should be placed on the back side o the support to align the specimen on the center of the supports. See Figure 1 for details.

6.1.1.4. *Loading Shaft*—A blunt-nosed loading shaft (with a spherical contact point 6.25 (±0.30) mm in radius) continuous with a load cell and a deflection measuring transducer which is capable of applying a contact load of 35 ±10 mN and maintaining a test load of 1961 ±50 mN and 4413 ±50 mN for the different temperature levels. The rise time for the test load shall be less than 0.5 s where the rise time is the time required for the load to rise from the 35 ±10 mN preload to the 1961 ±50 mN or 4413 ±50 mN test load. During the rise time the system shall dampen the test load after the first five seconds to a constant ±10 mN value.

6.1.1.5. *Load Cell*—A load cell with a minimum capacity of 9,806 mN having a minimum resolution of 2.5 mN mounted in-line with the loading shaft and above the fluid to measure the contact load and the test load.

6.1.1.6. *Linear Variable Differential Transducer (LVDT)*—A linear variable differential transducer or other suitable mounted device mounted axially above the loading shaft capable of resolving a linear movement ≤0.15 μm with a range of at least 6 mm to measure the deflection of the test beam.

6.1.2. *Controlled-Temperature Fluid Bath*—A controlled temperature liquid bath capable of maintaining the temperature at all points within the bath between –36 and 0°C within ±0.1°C. Placing a cold specimen in the bath may cause the bath temperature to fluctuate ±0.2°C from the target test temperature; consequently, bath fluctuations of 0.2°C during isothermal conditioning shall be allowed.

6.1.2.1. *Bath Agitator*—A bath agitator for maintaining the required temperature homogeneity with agitator intensity such that the fluid current does not disturb the testing process and mechanical noise caused by vibrations is less than the resolution specified in Sections 6.1.3 and 6.1.3.1.

6.1.2.2. *Circulating Bath (Optional)*—A circulating bath unit separate from the test frame which pumps the bath fluid through the test bath. If used, vibrations from the circulating system shall be isolated from the bath test chamber so that mechanical noise is less than the resolution specified in Sections 6.1.3 and 6.1.3.1.

6.1.3. *Data Acquisition System*—A data acquisition system that resolves loads to the nearest 2.5 mN, beam deflection to the nearest 0.15 μm, and bath fluid temperature to the nearest 0.1°C. The system shall sense the point in time when the signal is sent to the solenoid valve(s) to switch from zero load regulator (contact load) to the testing load regulator (test load). This is zero time. Using this time as a reference, the system shall provide a record of load and deflection measurements relative to this time. The system shall record the load and deflection at the loading times of 0.0, 0.5, 8.0, 15.0, 30.0, 60.0, 120.0, and 240s. All readings shall be an average of three or more points within ±0.2 seconds from the loading time, e.g., for a loading time of 7.8, 7.9, 8.0, 8.1, and 8.2 seconds.

6.1.3.1. *Signal Filtering*—Digital or analog smoothing of the load and the deflection data may be required to eliminate electronic noise that could otherwise affect the ability of the second order polynomial to fit the data with sufficient accuracy to provide a reliable estimate of *m*-value. The load and deflection signals may be filtered with a low pass analog or digital filter that removes signals of greater than 4 Hz frequency. The averaging shall be over a time period less or equal to ±0.2 s of the reporting time.

6.2. *Temperature Measuring Equipment*—A calibrated temperature transducer capable of measuring the temperature to 0.1°C over the range of –36 to 0°C mounted within 50 mm of the midpoint of the test specimen supports.

Note 1—Required temperature measurement can be accomplished with an appropriately calibrated platinum resistance thermometer (RTD) or a thermistor. Calibrations of an RTD or thermistor can be verified as per Section 6.6. An RTD meeting DIN Standard 43760 (Class A) is recommended for this purpose. The required precision and accuracy cannot be obtained unless each RTD is calibrated as a system with its respective meter or electronic circuitry.

6.3. *Items for Calibration or Verification*—The following items are required to verify and calibrate the BBR.

6.3.1. *Stainless Steel (Thick) Beam for Compliance Measurement and Load Cell Calibration*—One stainless steel beam, 6.4 ±0.1 mm thick by 12.7 0.25 mm wide by 127 ±5 mm long, for measuring system compliance and calibrating the load cell.

6.3.2. *Stainless Steel (Thin) Beam for Overall System Check*—One stainless steel beam, 1.3 ± 0.3 mm thick by 12.7 ±0.1 mm wide by 127 ±5 mm long, with an elastic modulus reported to three significant figures by the manufacturer. The manufacturer shall measure and report the thickness of this beam to the nearest 0.01 mm and the width to the nearest 0.05 mm. The dimensions of the beam shall be used to calculate the modulus of the beam during the overall system check. See Section 10.1.2.1.

6.4. *Standard Masses*—One or more standard masses are required as follows:

6.4.1. *Verification of Load Cell Calibration*—One or more masses totaling 100 ±0.2 g and two masses of 2 ±0.2 g each (see Note 3) for verifying the calibration of the load cell.

Note 3—A coin may be used if the mass is confirmed to be 2 ± 0.2 g.

6.4.2. *Calibration of Load Cell*—Four masses, each of known mass ±0.2 g, and equally spaced in mass over the range of the load cell.

6.4.3. *Daily Overall System Check*—Two or more masses, each of known mass to 0.2 g, for conducting overall system check as specified by the manufacturer.

6.4.4. *Accuracy of Masses*—Accuracy of the masses in Section 6.5 shall be verified at least once each every three years.

6.5. *Calibrated Thermometers*—Calibrated liquid-in-glass thermometers for verification of the temperature transducer of suitable range with subdivisions of 0.1°C. These thermometers shall be partial immersion thermometers with an ice point and shall be calibrated in accordance with

Test Method E 77 at least once per year. A suitable thermometer is designated 133C. An electronic thermometer of equal accuracy and resolution may be used.

6.6. *Thickness Gauge*—A stepped thickness gauge for verifying the calibrations of displacement transducer as described in Figure 3.

7. MATERIALS

7.1. *Bath Fluid*—A bath fluid that is not absorbed by or does not affect the properties of the asphalt mixture tested. The mass density of the fluid bath shall not exceed 1.05 kg/m3 at testing temperatures. The bath fluid shall be optically clear at all testing temperatures.. Silicone fluids or mixtures containing silicones shall not be used.

Note 4— Suitable bath fluids include ethanol, methanol, and glycol-methanol mixtures (e.g., 60 percent glycol, 15 percent methanol, 25 percent water).

8. HAZARDS

8.1. Observe standard laboratory safety procedures when handling hot asphalt binder and preparing test specimens.

8.2. Alcohol baths are flammable and toxic. Locate the controlled temperature bath in a well ventilated area away from sources of ignition. Avoid breathing alcohol vapors, and contact of the bath fluid with the skin.

8.3. Contact between the bath fluid and skin at the lower temperatures used in this test method can cause frostbite.

9. PREPARATION OF APPARATUS

9.1. Clean the supports, loading head and bath fluid of any particulates and coatings as necessary.

Note 5—Because of the brittleness of asphalt mixtures at the specified test temperatures, small fragments of asphalt mixtures can be introduced into the bath fluid. If these fragments are present on the supports or the loading head, the measured deflection will be affected. The small fragments, because of their small size, will deform under load and add an apparent deflection of the beam. Filtration of the bath fluid will aid in preserving the required cleanliness.

9.2. Select the test temperature and adjust the bath fluid to the selected temperature. Wait until the temperature stabilizes and then allow the bath to equilibrate to the test temperature ±0.1°C prior to conducting a test.

9.3. Activate the data acquisition system and load the software as explained in the manufacturer's manual for the test system.

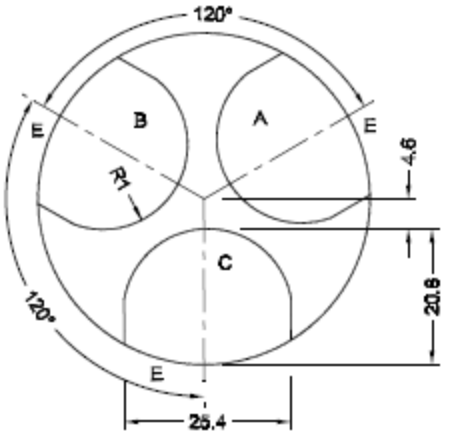

Top View

Note: Smooth Edges

Note: Sections A, B, and C are depressions with depths from the top surface as follows:

A 1.00 mm (0.0394") ± 0.01 mm

B 3.00 mm (0.1181")

C 6.00 mm (0.2362")

Hole Sizes:

D 4 mm dia x 7.0 mm deep, Counterbore 6 mm dia x 0.8 mm deep

E Depression, 2.4 mm Ball End Mill, 1.52 mm deep. Three places in-line with corresponding top surface depressions.

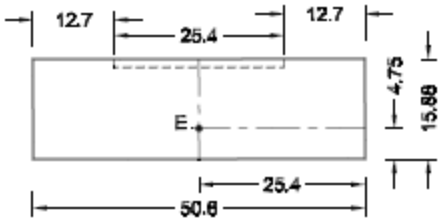

Front View

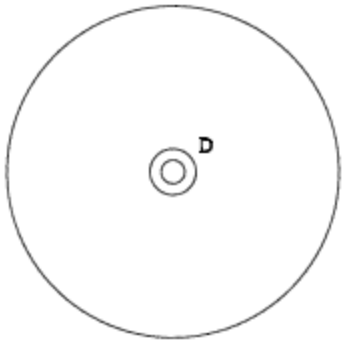

Bottom View

Note: 1. Bottom surface is flat and parallel with top surface
2. All dimensions are in millimeters unless otherwise indicated.

Figure 2—Typical Thickness Gauge Used to Calibrate Deflection Detector

10. STANDARDIZATION

10.1. Verify the calibration of the displacement transducer, load cell, and temperature transducer as described in Sections 10.1.1 through 10.1.6. As a minimum, each of the verification steps and

their frequency of performance shall be performed as described in this section. Additional verification steps may be performed at the recommendation of the manufacturer. Calibration procedures are described in the Annex. At the option of the manufacturer, the verification and calibration steps may be combined.

10.1.1. *Verification of Temperature Transducer*—On each day, before conducting tests, and whenever the test temperature is changed, verify calibration of the temperature detector by using a calibrated thermometer as described in Section 6.5. With the loading frame placed in the liquid bath, immerse the thermometer in the liquid bath close to the temperature transducer, and compare the temperature indicated by the thermometer to the temperature displayed by the data acquisition system. If the temperature indicated by the data acquisition system does not agree with the thermometer within ± 0.1°C, calibration is required.

10.1.2. *Verification of Freely Operating Air Bearing*—On each day, before conducting tests, verify that the air bearing is operating freely and is free of friction. Sections 10.1.2.1 and 10.1.2.2 shall be used to verify that the shaft is free of friction. If the requirements of Sections 10.1.2.1 and 10.1.2.2 are not satisfied, friction is present in the air bearing. Clean the shaft, and adjust the clearance of the displacement transducer as per the manufacturer's instructions. If this does not eliminate the friction, discontinue use of the BBR, and consult the manufacturer.

Note 6—Friction may be caused by a poorly adjusted displacement transducer core that rubs against its housing, an accumulation of asphalt binder on the loading shaft, by oil or other particulates in the air supply, and other causes.

10.1.2.1. Place the thin steel beam (Section 6.3.2) on the sample supports, and apply a 35 ±10 mN load to the beam using the zero load regulator. Observe the reading of the LVDT as indicated by the data acquisition system. Gently grasp the shaft, and lift it upwards approximately 5 mm by observing the reading of the LVDT. When the shaft is released, it shall immediately float downward and make contact with the beam.

10.1.2.2. Remove any beams from the supports. Use the zero load regulator to adjust the loading shaft so that it is free floating at the approximate midpoint of its vertical travel. Gently add a 2 g mass to the loading shelf. The shaft shall slowly drop downward under the mass.

10.1.3. *Verification of Displacement Transducer*—On each day, before conducting tests, verify the calibration of the displacement transducer using a stepped gauge block of known dimensions similar to the one shown in Figure 2. With the loading frame mounted in the bath at the test temperature, remove all beams from the supports, and place the gauge block on a reference platform underneath the loading shaft according to the instructions supplied by the instrument manufacturer. Apply a 100 g ± 0.2 g mass to the loading shaft, and measure the rise of the steps with the displacement transducer. Compare the measured values as indicated by the data acquisition system with the known dimensions of the gauge. If the known dimensions as determined from the gauge block and the dimensions indicated by the data acquisition system differ by more than ±5 μm, calibration is required. Perform the calibration, and repeat Section 10.1.1. If the requirements of Section 10.1.1 cannot be met after calibration, discontinue use of the device, and consult the manufacturer.

10.1.4. *Daily Overall System Check*—On each day, before conducting tests and with the loading frame mounted in the bath, perform a check on the overall operation of the system. Place the 1.3 ±0.3 mm thick stainless steel (thin) beam of known modulus as described in Section Section 6.3.2on the sample supports. Following the instructions supplied by the manufacturer, place the beam on the supports and apply a 50.0 or 100.0 ±0.2 g initial mass (491 or 981 mN ±2 mN) to the beam to ensure that the beam is seated and in full contact with the supports. Following the manufacturer's instructions, apply a second additional load of 100.0 to 300.0±0.2 g to the

beam. The software provided by the manufacturer shall use the change in load and associated change in deflection to calculate the modulus of the beam to three significant figures. The modulus reported by the software shall be within 10 percent of the modulus reported by the manufacturer of the beam; otherwise, the overall operation of the BBR shall be considered suspect and the manufacturer shall be consulted

10.1.5. *Verification of Load Cell*—Verify the calibration of the load cell as follows:

10.1.5.1. *Contact Load*—On each day, verify the calibration of the load cell in the range of the contact load. Place the 6.3 mm thick stainless steel compliance beam (Section 6.3.1) on the supports. Apply a 20 ±10 mN load to the beam using the zero load pressure regulator. Add the 2.0±0.2g mass as specified in Section 6.5.1 to the loading platform. The increase in the load displayed by the data acquisition system shall be 20 ±5 mN. Add a second 2.0 ± 0.2 g mass to the loading platform. The increase in the load displayed by the data acquisition system shall be 20 ±5 mN. If the increases in displayed load are not 20 ±5 mN, calibration is required. Perform the calibration. If the requirements of Section 10.1.3.1 cannot be met after calibration, discontinue use of the device, and consult the manufacturer.

10.1.5.2. *Test Load*—On each day, before conducting tests, verify the calibration of the load cell in the range of the test load. Place the 6.3 mm thick stainless steel compliance beam (Section 6.4.1) on the supports. Use the zero load regulator (contact load) to apply a 20 ±10 mN load to the beam. Add the 100 g mass to the loading platform. The increase in the load displayed by the data acquisition system shall be 981 ±5 mN. Otherwise, calibrate the load cell. If the requirements of Section 10.1.3.2 cannot be met after calibration, discontinue use of the device, and consult the manufacturer.

10.1.6. *Verification of Front-to-Back Alignment of Loading Shaft*—Every six months, check the alignment of the loading shaft with the center of the sample supports with an alignment gauge supplied by the manufacturer or by measurement as follows: Cut a strip of white paper about 25 mm in length and slightly narrower than the width of the compliance beam. Stick the paper strip to the center of the compliance beam with tape. Move the frame out of the bath, place the compliance beam on the supports, and place a small section of carbon paper over the paper. With the air pressure applied to the air bearing, push the shaft downward causing the carbon paper to make an imprint on the white paper. Remove the beam, and measure the distance from the center of the imprint to each edge of the beam with a pair of vernier calipers. The difference between the two measurements shall be 1.0 mm or less. If this requirement is not met, contact the manufacturer of the device.

11. PREPARATION OF TEST SPECIMENS

11.1. Tall Gyratory Cylinder (170 ±2 mm height by 150 mm diameter) - Asphalt mixture BBR beams are obtained from gyratory compacted specimens (11.2. and 11.3.) and from field cores (11.4.). See AASHTO T 312-09 for the preparation of cylindrical gyratory mixtures specimen.

11.1. 1 This method is used when other tests, such as IDT (AASHTO R 322-07) are performed and a comprehensive direct comparison of the BBR and IDT results is needed.

11.1.2. Step 1 - The top 15 mm and the bottom 15 mm of the gyratory specimen are removed using a typical laboratory saw for mixture specimen preparation to obtain smooth surfaces. The remaining cylinder is cut into three 40 mm-thick IDT specimens, which may be tested at three different temperatures (each at one temperature) to determine the mixture creep compliance (Figure 3).

11.1.3. Step 2 - One day after IDT creep testing is completed (if performed), the specimens are further cut to obtain BBR thin beams. First, a thin slice, approximately 5 mm thick, is cut from one face of the IDT specimen to ensure a smooth surface and to remove any glue remaining from IDT buttons. Next, a 12.5 mm thick slice is cut from the remaining part of the IDT specimen, see Figure 4. This slice is used in the next two steps to prepare the BBR beams. Note that the remaining 17-18 mm part at the bottom of

the IDT specimen is necessary to hold the IDT specimen during saw cutting (see Figure 4) to remove the first thin layer and then accurately cut the next slice used for the BBR beams.

11.1.4. Step 3 - The 12.5 mm thick slice is further cut from three sides to obtain 122 mm wide irregular slice, as shown in Figure 5.

11.1.5. Step 4. The slice obtained in step 3 is further cut into approximately 11 beams depending on the saw blade thickness, as shown in Figure 6. Each beam should have a size of 6.35 ± 0.05-mm thick by 12.70 ±0.05-mm wide by 127 ±2.0-mm long. Thickness and width of each beam should be measured in three points by mean of a caliper and the average reported and input in the software of the machine. A simple tile saw can be used to produce BBR mixture beams with uniform dimension. The blade has to present a continuous rim. The direction used to cut the thin beams with respect to the IDT specimens loading direction is not significant.

11.2. Normal Gyratory Cylinder (115 ±5 mm height by 150 mm diameter)

11.2.1. If IDT samples are required, then step 11.1.2. is modified as follows: the top 10 mm and the bottom 10 mm of the gyratory specimen are removed and the remaining cylinder is cut into two 40 mm-thick IDT specimens. The remaining steps do not change.

11.2.2. If other mechanical tests are not required, then step 11.1.2. is modified as follows: the top 45 mm of the gyratory is removed and a 12.5 mm thick slice is cut from the remaining cylinder; this slice represents the middle portion of the original gyratory specimen. The remaining steps do not change.

11.3. Field Cores - The cores should be cut into slices following the procedure previously described 11.1. and 11.2., taken into consideration that typical lift thickness is 50.8 mm (2 in.) Particular attention should be given to the core surface; for very rough surfaces, the top 5 mm may have to be removed; for reasonable smooth surfaces, the top can be kept since it represents the most aged portion of the asphalt pavement

12. PROCEDURE

12.1. Two test temperature levels can be used for testing with the following loads respectively:
1961 mN at high temperature level = low temperature grade of binder + 10˚C + 12˚C, and 4413 mN at intermediate temperature level = low temperature grade of binder + 10˚C. For the low temperature level = low temperature grade of binder + 10˚C - 12˚C, it is recommended to predict the stiffness curve by applying time-temperature superposition principle to the experimental data at the intermediate and high temperature levels.

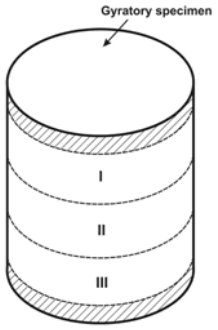

Figure 3— Cutting BBR mixture beams: Step 1

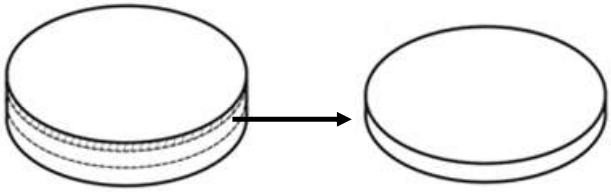

Figure 4— Cutting BBR mixture beams: Step 2

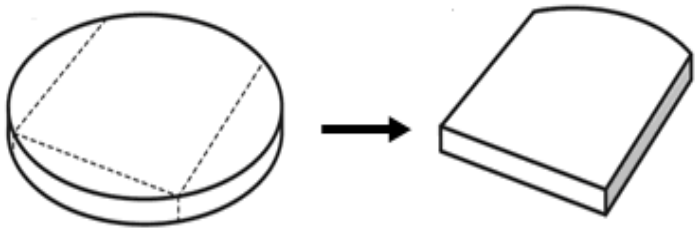

Figure 5— Cutting BBR mixture beams: Step 3

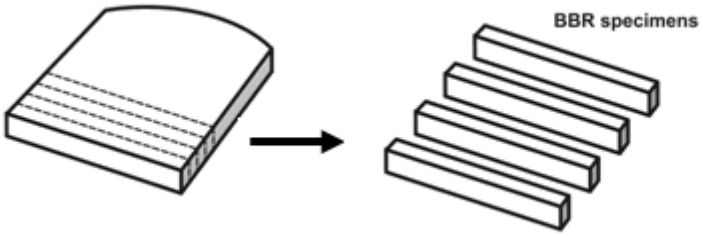

Figure 6— BBR mixture beams: Step 4

12.1.1. Place the test specimen in the testing bath and condition it at the testing temperature for 60 ±5 minutes.

Note 7—Asphalt binders may harden rapidly when held at low temperatures. This effect, which is called physical hardening, is reversible when the asphalt binder is heated to room temperature or slightly above. Because of physical hardening, conditioning time must be carefully controlled if repeatable results are to be obtained.

12.2. *Checking Contact Load and Test Load*—Check the adjustment of the contact load and test load prior to testing each set of test specimens. The 6.35-mm thick stainless steel beam shall be used for checking the contact load and test load.

Note 8—Do not perform these checks with the thin steel beam or an asphalt test specimen.

12.2.1. Place the thick steel beam in position on the beam supports. Using the test load regulator valve, gently increase the force on the beam to 1961 ±50 mN or 4413 ±50 mN test load.

12.2.2. Switch from the test load to the contact load, and adjust the force on the beam to 35 ± 10 mN. Switch between the test load and contact load four times.

12.2.3. When switching between the test load and contact load, watch the loading shaft and platform for visible vertical movement. The loading shaft shall maintain contact with the steel beam when switching between the contact load and test load while maintaining these loads at 35 ± 10 mN and 1961 ±50 mN or 4413 ±50 mN test load, respectively.

12.2.4. *Corrective Action*—If the requirements of Sections 12.2.1 to 12.2.3 are not met, the device may require calibration as per the manufacturer's instructions or the loading shaft may be dirty or require alignment (see Section 10.1.2). If the requirements of Sections 12.2.1 to 12.2.3 cannot be met after calibration, cleaning, or other corrective action, discontinue use of the device and consult the equipment manufacturer.

12.3. Enter the specimen identification information, test load, test temperature, time the specimen is placed in the bath at the test temperature, and other information as appropriate into the computer which controls the test system.

12.4. After conditioning, place the test beam on the test supports, and initiate the loading sequence of the test. Maintain the bath at the test temperature ±0.1°C during testing; otherwise, the test shall be rejected.

12.5. Manually apply a 35 ± 10 mN contact load to the beam to ensure contact between the beam and the loading head for no more than 10 s. The specified contact load is required to ensure continuous contact between the loading shaft and support, and the specimen. Failure to establish continuous contact within the required load range gives misleading results. The contact load shall be applied by gently increasing the load to 35 ± 10 mN. While applying the contact load, the load on the beam shall not exceed 45 mN, and the time to apply and adjust the contact load shall be no greater than 10 s.

12.6. *Activate the automatic test system that is programmed to proceed as follows*:

12.6.1. Immediately after the application of the 35 mN contact load, increase the load from 35 ± 10 mN to the 1961 ±50 mN or 4413 ±50 mN seating load for 1.0 ±0.1 s for high and for intermediate and low temperature levels respectively seating load for 1.0 ±0.1 s.

Note 9—The seating loads described in Sections 12.6.1 and 12.6.2 are applied and removed automatically by the computer-controlled loading system and are transparent to the operator. Data are not recorded during the initial loading.

12.6.2. Reduce the load to 35 ±10 mN and allow the beam to recover for 20.0 ±0.1 s.

12.6.3. Apply a test load ranging as specified in Section 6.1.1.2.

Note 10—The actual load on the beam as measured by the load cell is used in calculating the stress in the beam. The initial seating and test load includes the 35 ±10 mN preload.

Note 11—Modifications of the BBR software by the manufacturer increased the resolution of deflection measurements; the latest hardware and software can resolve deflections of 0.15 microns with an accuracy of less than 1 micron

12.6.4. Remove the test load and terminate the test.

12.6.5. At the end of the initial seating load, and at the end of the test, monitor the computer screen to verify that the load on the beam returns to 35 ±10 mN in each case. If the beam does not return to 35 ±10 mN, the test is invalid and the rheometer should be calibrated.

12.7. Remove the specimen from the supports and proceed to the next test.

13. CALCULATION AND INTERPRETATION OF RESULTS

13.1. See Annex.

14. REPORT

14.1. *Report data as shown in Figure 4 that describes individual test, including*:

14.1.1. Maximum and minimum temperature of the test bath measured during the 240 seconds of testing measured at 1.0 second interval to the nearest 0.1°C,

14.1.2. Date and time when test load is applied,

14.1.3. File name of test data,

14.1.4. Name of operator,

14.1.5. Sample identification number,

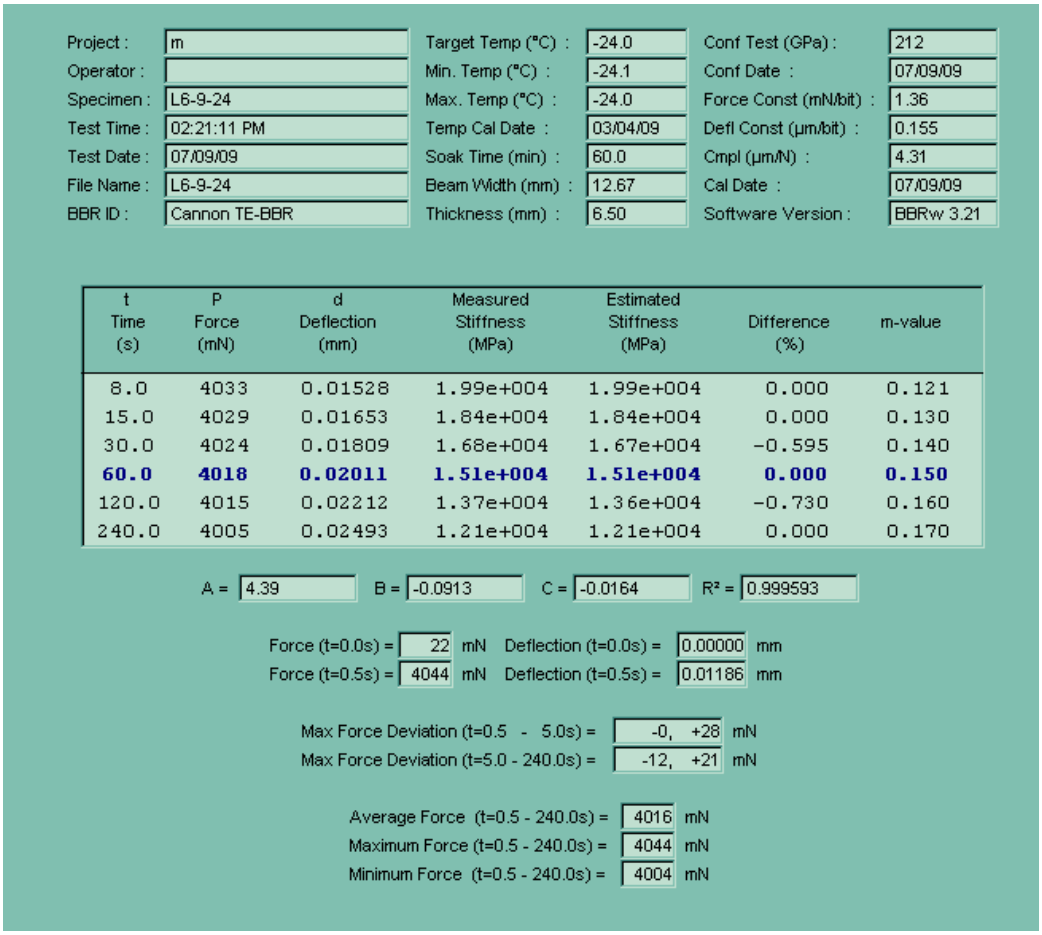

Project :	m	Target Temp (°C) :	-24.0	Conf Test (GPa) :	212	
Operator :		Min. Temp (°C) :	-24.1	Conf Date :	07/09/09	
Specimen :	L6-9-24	Max. Temp (°C) :	-24.0	Force Const (mN/bit) :	1.36	
Test Time :	02:21:11 PM	Temp Cal Date :	03/04/09	Defl Const (µm/bit) :	0.155	
Test Date :	07/09/09	Soak Time (min) :	60.0	Cmpl (µm/N) :	4.31	
File Name :	L6-9-24	Beam Width (mm) :	12.67	Cal Date :	07/09/09	
BBR ID :	Cannon TE-BBR	Thickness (mm) :	6.50	Software Version :	BBRw 3.21	

t Time (s)	P Force (mN)	d Deflection (mm)	Measured Stiffness (MPa)	Estimated Stiffness (MPa)	Difference (%)	m-value
8.0	4033	0.01528	1.99e+004	1.99e+004	0.000	0.121
15.0	4029	0.01653	1.84e+004	1.84e+004	0.000	0.130
30.0	4024	0.01809	1.68e+004	1.67e+004	-0.595	0.140
60.0	**4018**	**0.02011**	**1.51e+004**	**1.51e+004**	**0.000**	**0.150**
120.0	4015	0.02212	1.37e+004	1.36e+004	-0.730	0.160
240.0	4005	0.02493	1.21e+004	1.21e+004	0.000	0.170

A = 4.39 B = -0.0913 C = -0.0164 R^2 = 0.999593

Force (t=0.0s) = 22 mN Deflection (t=0.0s) = 0.00000 mm
Force (t=0.5s) = 4044 mN Deflection (t=0.5s) = 0.01186 mm

Max Force Deviation (t=0.5 - 5.0s) = -0, +28 mN
Max Force Deviation (t=5.0 - 240.0s) = -12, +21 mN

Average Force (t=0.5 - 240.0s) = 4016 mN
Maximum Force (t=0.5 - 240.0s) = 4044 mN
Minimum Force (t=0.5 - 240.0s) = 4004 mN

Figure 4—Typical Test Report

14.1.6. Time beam in bath,

14.1.7. Time test started,

14.1.8. Any flags issued by software during test,

14.1.9. Correlation coefficient, R^2 for log stiffness versus log time, expressed to nearest 0.000001,

14.1.10. Anecdotal comments (maximum 256 characters),

14.1.11. Report constants A, B, and C to three significant figures,

14.1.12. Difference between measured and estimated stiffness calculated as:
(Estimated – Measured) ×100 percent/Measured.

14.2. Report load and deflection as for times 0.0 and 0.5 seconds.

14.3. Report data as shown in Figure 4 for time intervals of 8.0, 15.0, 30.0, 60.0, 120.0, and 240 seconds including:

14.3.1. Loading time, nearest 0.1 second;

14.3.2. Load, nearest 1.0 mN;

14.3.3. Beam deflection, nearest 1 μm;

14.3.4. Measured Stiffness modulus, MPa, expressed to three significant figures;

14.3.5. Estimated Stiffness Modulus, MPa, expressed to three significant figures;

14.3.6. Difference between measured and estimated Stiffness Modulus in percent;

14.3.7. Estimated *m*-value, nearest 0.001; and

14.3.8. Regression Coefficients and least square fit R_2 value.

15. PRECISION AND BIAS

15.1. *Precision*—Criteria for judging the acceptability of creep stiffness and slope results obtained by this method are given in Table 1.

15.1.1. *Single-Operator Precision (Repeatability)*—The figures in Column 2 of Table 1 are the coefficients of variation that have been found to be appropriate for the conditions of test described in Column 1. Two results obtained in the same laboratory, by the same operator using the same equipment, in the shortest practical period of time, should not be considered suspect unless the difference in the two results, expressed as a percent of their mean, exceeds the values given in Table 1, Column 3.

15.1.2. *Multilaboratory Precision (Reproducibility*—The figures in Column 2 of Table 1 are the coefficients of variation that have been found to be appropriate for the conditions of test described in Column 1. Two results submitted by two different operators testing the same material in different laboratories shall not be considered suspect unless the difference in the two results, expressed as a percent of their mean, exceeds the values given in Table 1, Column 3.

Table 1—Precision Estimates

Condition	Coefficient of Variation (1s%)[a]	Acceptable Range of Two Test Results (d2s%)[a]
Single-Operator Precision:		
Creep Stiffness (MPa)	2.5	7.2
Slope (*m*-value)	1.0	2.9
Multilaboratory Precision:		
Creep Stiffness (MPa)	6.3	17.8
Slope (*m*-value)	2.4	6.8

[a] These values represent the 1s% and d2s% limits described in ASTM Practice C 670.

Note 18—The precision estimates given in Table 1 are based on the analysis of test results from eight pairs of AMRL proficiency samples. The data analyzed consisted of results from 174 to 196 laboratories for each of the eight pairs of samples. The analysis included five binder grades: PG 52-34, PG 64-16, PG 64-22, PG 70-22, and PG 76-22 (SBS modified). Average creep stiffness results ranged from 125.4 MPa to 236.8 MPa. Average slope results ranged from an *m*-value of 0.308 to 0.374. The details of this analysis are in the final report for NCHRP Project No. 9-26, Phase 3.

Note 19—As an example, two tests conducted on the same material yield creep stiffness results of 190.3 MPa and 200.7 MPa, respectively. The average of these two measurements is 195.5 MPa. The acceptable range of results is then 7.2 percent of 195.5 MPa or 14.1 MPa. As

the difference between 190.3 MPa and 200.7 MPa is less than 14.1 MPa, the results are within the acceptable range.

15.2. *Bias*—No information can be presented on the bias of the procedure because no material having an accepted reference value is available.

16. KEYWORDS

16.1. Flexural; creep stiffness; flexural creep compliance; bending beam rheometer.

ANNEX

(Mandatory Information)

A1.1 *Calibration of Displacement Transducer*—Calibrate the displacement transducer using a stepped gauge block of known dimensions similar to the one shown in Figure 3. With the loading frame mounted in the bath at the test temperature, remove all beams from the supports, and place the stepped gauge block on a reference platform underneath the loading shaft according to the instructions supplied by the instrument manufacturer. Apply a 100-g mass on the loading shaft, and follow the manufacturer's instructions to obtain a displacement transducer reading on each step. The software provided by the manufacturer shall convert the measurements to a calibration constant in terms of μm/bit to three significant figures and shall automatically enter the new constant into the software. The calibration constant should be repeatable within 10 percent from one calibration to another; otherwise, the operation of the system may be suspect.

A1.2 *Calibration of Load Cell*—Calibrate the load cell in accordance with the manufacturer's instructions using a minimum of four masses evenly distributed over the range of the load cell.

The software provided by the manufacturer shall convert the measurements to a calibration constant in terms of mN/bit to three significant figures and shall automatically enter the new constant into the software. The calibration constants should be repeatable within 10 percent from one calibration to another; otherwise, the operation of the system may be suspect. Repeat the process for each test temperature.

A1.3 *Calibration of Temperature Transducer*—Calibrate the temperature detector by using a calibrated thermometer of suitable range meeting the requirements of Section 10.1.5. Immerse the thermometer in the liquid bath close to the thermal detector, and compare the temperature indicated by the calibrated thermometer to the detector signal being displayed. If the temperature indicated by the thermal detector does not agree with the thermometer within ±0.1°C, follow the manufacturer's instructions for correcting the displayed temperature to agree with the thermometer temperature.

A1.4 *Determine the System Compliance*—Determine the system compliance in accordance with the manufacturer's instructions using a minimum of four masses evenly distributed over the range of the load cell. The data acquisition software shall measure the position of the displacement transducer at each load. The compliance shall be calculated as the measured deflection per unit load. The software provided by the manufacturer shall convert the measurements to a compliance in terms of μm/N to three significant figures and shall automatically enter the compliance into the software. The compliance measurement may be performed as part of the load cell calibration or as a separate operation. The compliance measurement shall be performed each time the load cell is calibrated. The compliance value should be repeatable within 10 percent from one determination to another; otherwise, the operation of the system may be suspect. Repeat the process for each test temperature.

A1.5 *Typical Test Result*—A typical test result is shown in Figure 4. Disregard measurements obtained and the curves projected on the computer screen during the initial eight seconds of the application of the test load. Data from a creep test obtained immediately after the application of the test load may not be valid because of dynamic loading effects and the finite rise time. Use only the data obtained between 8 and 240s loading time for calculating $S(t)$ and m.

A1.6 *Deflection of an Elastic Beam*—Using the elementary bending theory, the mid-span deflection of an elastic prismatic beam of constant cross-section loaded in three-point loading can be obtained by applying Equations A1.1 and A1.2 as follows:

$$\delta = PL^3/48EI \qquad (A1.1)$$

where:
δ = deflection of beam at midspan, mm;
P = load applied, N;
L = span length, mm;
E = modulus of elasticity, MPa; and
I = moment of inertia, mm^4.
and:

$$I = bh^3/12 \qquad (A1.2)$$

where:
I = moment of inertia of cross-section of test beam, mm^4;
b = width of beam, mm; and
h = thickness of beam, mm.

Note A1—The test specimen has a span to depth ratio of 16:1 and the contribution of shear to deflection of the beam can be neglected.

A1.7 *Elastic Flexural Modulus*—According to elastic theory, calculate the flexural modulus of a prismatic beam of constant cross-section loaded at its midspan using the following equation:

$$E = PL^3/4bh^3\delta \quad (A1.3)$$

where:
E = time-dependent flexural creep stiffness, MPa;
P = constant load, N;
L = span length, mm;
b = width of beam, mm;
h = thickness of beam, mm; and
δ = deflection of beam, mm.

A1.8 *Maximum Bending Stress*—The maximum bending stress in the beam occurs at the midspan at the top and bottom of the beam. Calculate σ thus:

$$\sigma = 3PL/2bh^2 \quad (A1.4)$$

where:
σ = maximum bending stress in beam, MPa;
P = constant load, N;
L = span length, mm;

b = width of beam, mm; and
h = thickness of beam, mm.

A1.9 *Maximum Bending Strain*—The maximum bending strain in the beam occurs at the midspan at the top and bottom of the beam. Calculate ϵ using the following equation:

$$\epsilon = 6\delta h/L^2 \text{ mm/mm} \quad (A1.5)$$

where:
ϵ = maximum bending strain in beam, mm/mm;
δ = deflection of beam, mm;
h = thickness of beam, mm; and
L = span length, mm.

A1.10 *Linear Viscoelastic Stiffness Modulus*—According to the elastic-viscoelastic correspondence principle, it can be assumed that if a linear viscoelastic beam is subjected to a constant load applied at $t = 0$ and held constant, the stress distribution is the same as that in a linear elastic beam under the same load. Further, the strains and displacements depend on time and are derived from those of the elastic case by replacing E with $1/D(t)$. Since $1/D(t)$ is equivalent to $S(t)$, rearranging the elastic solution results in the following relationship for the stiffness:

$$S(t) = PL^3/4bh^3\delta(t) \quad (A1.6)$$

where:
$S(t)$ = time-dependent flexural creep stiffness, MPa;
P = constant load, N;
L = span length, mm;
b = width of beam, mm;
h = thickness of beam, mm;
$\delta(t)$ = deflection of beam, mm; and
$\delta(t)$ and $S(t)$ indicate that the deflection and stiffness, respectively, are functions of time.

A1.11 *Presentation of Data*:

A1.11.1 Plot the response of the test beam to the creep loading as the logarithm of stiffness with respect to the logarithm of loading time. A typical representation of test data is shown in Figure 4. Over the limited testing time from 8 to 240 seconds, the plotted data shown in Figure A1.1 can be represented by a second order polynomial as follows:

$$\log S'(t) = A + B[\log(t)] + C[\log(t)]^2 \quad (A1.7)$$

and, the slope, m, of the logarithm of stiffness versus logarithm time curve is equal to (absolute value):

$$|m(t)| = d[\log S'(t)]/d[\log(t)] = B + 2C[\log(t)] \quad (A1.8)$$

where:

$S'(t)$ = time-dependent flexural creep stiffness estimated using Equation A1.7, MPa;

T = time in seconds; and

A, B, and C = regression coefficients.

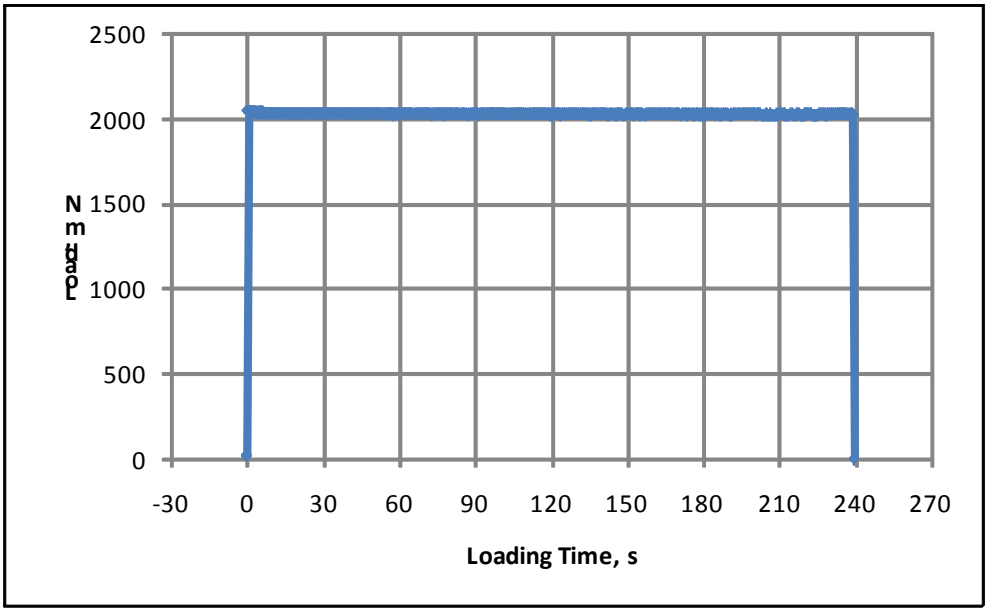

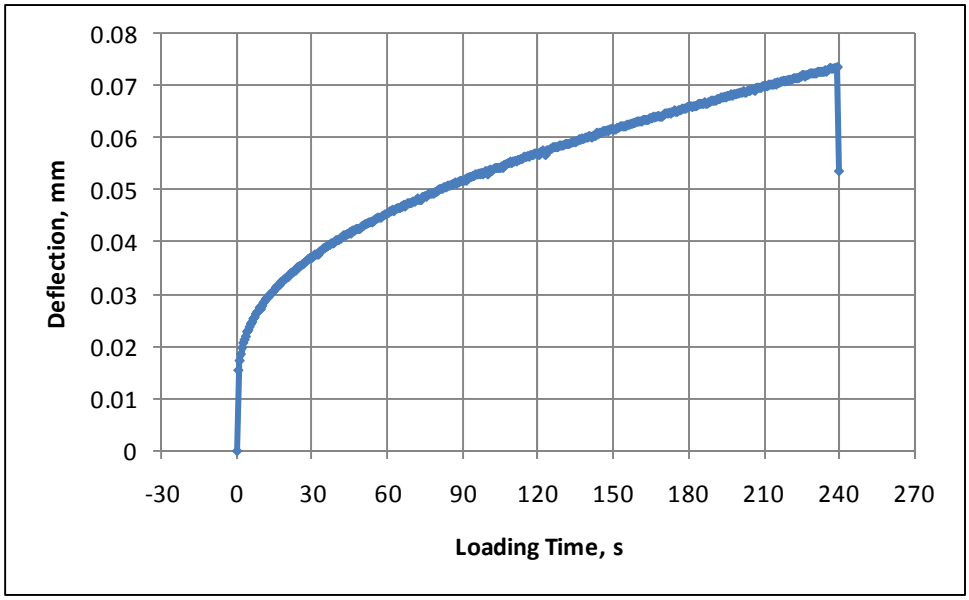

Figure A1.1—Typical Load and Deflection Plots

A1.11.2 Smoothing the data may be required to obtain smooth curves for the regression analysis as required to determine an *m*-value. This procedure can be performed by averaging five readings taken at the reported time ± 0.1 and ±0.2 s.

A1.11.3 Obtain the constants *A*, *B*, and *C* from the least squares fit of Equation A1.7. Use data equally spaced with respect to the logarithm of time to determine the regression coefficients in Equations A1.7 and A1.8. Determine experimentally the stiffness values used for the regression to derive the coefficients *A*, *B*, and *C* and to, in turn, calculate values of *m* after loading times of 8, 15, 30, 60, 120, and 240 s.

A1.12 Calculation of regression coefficients, estimated stiffness values, and *m*:

A1.12.1 Calculate the regression coefficients *A*, *B*, and *C* in Equations A1.7 and A1.8 and the denominator *D* as follows:

$$A = S_y(S_{x2}S_{x4} - S_{x3}^2) - S_{xy}(S_{x1}S_{x4} - S_{x2}S_{x3}) + S_{xxy}(S_{x1}S_{x3} - S_{x2}^2)]/D \quad (A1.9)$$

$$B = [6(S_{xy}S_{x4} - S_{xxy}S_{x3}) - S_{x1}(S_yS_{x4} - S_{xxy}S_{x2}) + S_{x2}(S_yS_{x3} - S_{xy}S_{x2})]/D \quad (A1.10)$$

$$C = [6(S_{x2}S_{xxy} - S_{x3}S_{xy}) - S_{x1}(S_{x1}S_{xxy} - S_{x3}S_y) + S_{x2}(S_{x1}S_{xy} - S_{x2}S_y)]/D \quad (A1.11)$$

$$D = 6(S_{x2}S_{x4} - S_{x3}^2) - S_{x1}(S_{x1}S_{x4} - S_{x2}S_{x3}) + S_{x2}(S_{x1}S_{x3} - S_{x2}^2) \quad (A1.12)$$

where, for loading times of 8, 15, 30, 60, 120, and 240 seconds:
$S_{x1} = \log 8 + \log 15 + \ldots \log 240$;
$S_{x2} = (\log 8)^2 + (\log 15)^2 + \ldots (\log 240)^2$;
$S_{x3} = (\log 8)^3 + (\log 15)^3 + \ldots (\log 240)^3$;
$S_{x4} = (\log 8)^4 + (\log 15)^4 + \ldots (\log 240)^4$;
$S_y = \log S(8) + \log S(15) + \ldots \log S(1000)$;
$S_{xy} = \log S(8)(\log (8)) + \log S(15) \log (15) + \ldots \log S(240) \log (240)$; and
$S_{xxy} = [\log (8)]^2 \log S(8) + [\log (15)]^2 \log S(15) + \ldots [\log (240)]^2 \log S(240)$.

A1.12.2 Calculate the estimated stiffness $S'(t)$ at 8, 15, 30, 60, 120, and 240 s as follows:

$$\log S'(t) = A + B[\log(t)] + C\,[\log(t)]^2 \qquad (A1.13)$$

A1.12.3 Calculate the estimated m-value at 8, 15, 30, 60, 120, and 240 s as the absolute value of

$$|m| = B + 2C\,[\log(t)] \qquad (A1.14)$$

A1.12.4 Calculate S the average of the stiffness values at 8, 15, 30, 60, 120, and 240 seconds as:

$$\log S = [\log S(8) + \ldots \log S(240)]/8 \qquad (A1.15)$$

A1.12.5 Calculate the fraction of the variation in the stiffness explained by the quadratic model as:

$$R^2 = 1.00 - \left[\frac{[\log S(8) - \log S'(8)] + \ldots [\log S(1000) - \log S'(1000)]}{[\log S(8) - \log(\overline{S})]^2 + \ldots [\log S(1000) - \log(\overline{S})]^2} \right] \qquad (A1.16)$$

A1.12.6 Use the estimated values of the stiffness and m at 60 s for specification purposes. Measured and estimated stiffness values should agree to within two percent. Otherwise, the test is considered suspect.